*NEUTRON DIFFRACTION STUDY OF MAGNETIC MATERIALS**

G. S. ZHDANOV and R. P. OZEROV

Usp. Fiz. Nauk 76, 239-282 (February, 1962)

CONTENTS

THE diffraction of x rays and electrons has been used to study the atomic structures of molecules, liquids, amorphous bodies, and especially crystals. The world of atomic structures of crystals obeys rigorous symmetry laws, discovered by E. S. Fedorov and has been shown by structural investigations to possess a wide range of structural defects, which are most essential to the understanding of the properties of real crystals. Neutron diffraction, while possessing all the main capabilities of x-ray and electron diffraction, has a special property, possessed by no other method, brought about by magnetic scattering of neutrons on the uncompensated electron spins of the atoms in molecules and crystals. Neutron diffraction studies have thus made it possible to probe the realm of magnetic structures, which is connected with the realm of atomic structures and at the same time has its own set of laws. Just as in ordinary crystalline materials the connection between the composition and the physical properties can be determined only by knowledge of the atomic structure, an understanding of the properties of magnetic materials is essentially dependent on a knowledge of the magnetic structure.

1. MAGNETIC SCATTERING OF NEUTRONS

Nuclear and magnetic scattering amplitudes. The scattering of neutrons by a substance depends primarily on the scattering ability of the atomic nuclei. The effective cross section for scattering by the nucleus of an atom with a fully compensated electron-shell magnetic moment is determined by the relation

$$d\sigma = b^2, \tag{1}$$

where b is the nuclear scattering amplitude, which is independent of the angle. If the atom has an uncompensated resultant spin moment S, additional magnetic scattering occurs, with a cross section

$$d\sigma = p^2, \tag{2}$$

where p is an angle-dependent magnetic scattering amplitude. This amplitude is given[1] by the formula

$$p = \left(\frac{e^2\gamma}{mc^2}\right) S f_m, \tag{3}$$

where e and m are the charge and mass of the electron, c the velocity of light, γ the neutron magnetic moment, and f_m an atomic scattering factor (form factor) which depends on the scattering angle, as in the case of x rays. Unlike the x-ray case, the factor f_m (Fig. 2) is determined by the distribution of not all the electrons of the atom, but only of the "magnetic" electrons, i.e., electrons with uncompensated spin. The magnetic scattering amplitude p is determined from spectroscopic or magnetic data. It varies with the valence states of the paramagnetic atoms and ions. For example, for Fe^{++} and Fe^{+++} the total spins are respectively S = 2 and $\frac{5}{2}$, which in turn determines the difference in p.

Scattering of neutrons by magnetic materials with ordered magnetic structure. If a polarized neutron beam having a definite neutron spin orientation in space passes through a ferromagnetic or antiferromagnetic crystal with parallel or antiparallel magnetic-moment orientation, then the nuclear and magnetic scattering are coherent and the resultant intensity of the neutron diffraction is determined by the orientation of the lattice relative to the crystal polarization and the neutron beam. Figure 1 shows one of the crystal reflecting planes, the orientation of which is specified by a unit scattering vector ϵ, parallel to the reciprocal lattice vector. Let **K** be a unit vector in the direction of the magnetic moment of the atom. A polarized neutron beam characterized by a

*This review is based on the paper "Magnetic Structures," delivered to the plenary Session of the Seventh Conference on the Application of X rays to the Study of Materials, June 19, 1961 (Leningrad).

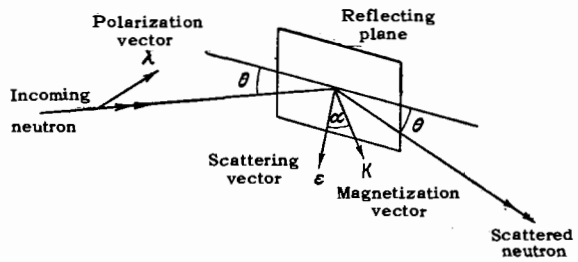

FIG. 1. Reflection of neutrons from the plane of a crystal with ordered magnetic structure.

unit polarization vector λ is incident on the crystal. The effective cross section for the scattering of neutrons by the atom is determined in this case by the Halpern and Johnson formula [2]

$$d\sigma = b^2 + 2bp(\mathbf{q}\lambda) + p^2q^2, \tag{4}$$

where $\mathbf{q}$ is the magnetic interaction vector

$$\mathbf{q} = \boldsymbol{\varepsilon}(\boldsymbol{\varepsilon}\mathbf{K}) - \mathbf{K}. \tag{5}$$

It is easy to see that the vector $\mathbf{q}$ lies in the plane of the vectors $\boldsymbol{\epsilon}$ and $\mathbf{K}$ and has an absolute value

$$q^2 = 1 - (\boldsymbol{\varepsilon}\mathbf{K})^2 = \sin^2\alpha, \tag{6}$$

where α is the angle between the scattering vector and the magnetization vector.

Paramagnetic ("gas") scattering. In a substance containing magnetic atoms having a resultant spin S and random spin orientation, the observed magnetic scattering will have an effective cross section per atom

$$d\sigma = \frac{2}{3}S(S+1)\left(\frac{e^2\gamma}{mc^2}\right)^2 f_m^2, \tag{7}$$

where the numerical coefficient $^2/_3$ is the mean value of q^2 for random spin orientation. As can be seen from (7), the intensity of scattering by paramagnetic atoms is the sum of two terms, one proportional to S^2 and the other proportional to S. The term with S^2 describes elastic neutron scattering, in which the spin orientation of the individual atoms does not change relative to that of the neighbors. This scattering is either diffuse or coherent, depending on the absence or presence of periodicity in the arrangement of the atomic magnetic moments. In a neutron-diffraction study of a substance at low temperatures, far from the Néel point T_a or the Curie point T_C, when the magnetic lattice is ordered, the intensities of the diffraction maxima are proportional to S^2. At temperatures above the magnetic-ordering temperature this scattering goes over into diffuse scattering with an intensity likewise proportional to S^2.

The term proportional to S describes the scattering cross section for which the orientation of the moments of individual atoms changes ("spin flip"). The rotation of the atomic magnetic moment is due to the work performed to overcome the exchange energy

$$A_{ij} = -2I_{ij}S_iS_j, \tag{8}$$

where S_i and S_j are the spin moments of two atoms, and I_{ij} the exchange integral. In this process the kinetic energy of the scattered neutron changes, and the scattering is inelastic. The cross section for scattering with spin flip depends in a complicated manner on the exchange energy or on the associated magnetic disorder temperature. If the exchange energy of the spins is less than the neutron energy, the term proportional to S is independent, in first approximation, of the specimen temperature.

Figure 2 shows the magnetic parts of the neutron scattering in the antiferromagnetic compounds MnF_2 (T_a = 75°K) and MnO (T_a = 120°K) at room temperature, corresponding to the paramagnetic state of these salts. In manganese difluoride, the magnetic-scattering curve is typically gas-like. We can determine from this curve the atomic magnetic factor for the manganese ion Mn^{++} (Fig. 3a). Comparison with the x-ray atomic factor discloses a faster attenuation, since the magnetoactive electrons are those of the 3d shell. The distribution of these electrons (Fig. 3b) is determined by taking the Fourier transform of the curve of Fig. 3a. The electron-density maxima on the experimental and theoretical curves of the 3d shell (~ 0.6 Å) lie close to each other.

The magnetic-scattering curve for MnO (Fig. 2) shows a reduction in intensity at low scattering angles, which is a characteristic of condensed systems in the case of x-ray scattering. This indicates conservation of partial magnetic ordering (short-range order regions) above the magnetic transformation point.

Scattering by magnetized crystals. To determine the magnetic form factor f_m it is necessary to determine the magnetic scattering amplitude p. For an

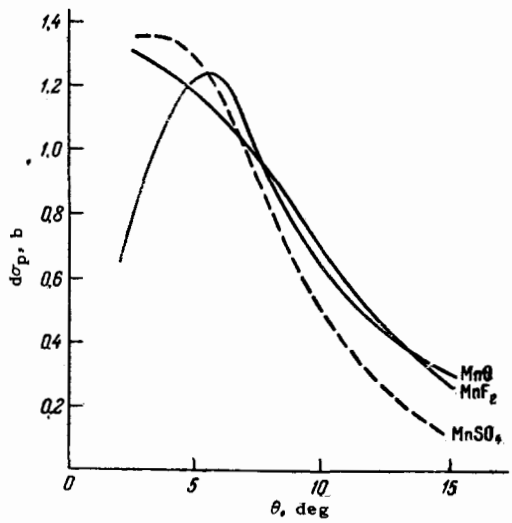

FIG. 2. Magnetic scattering in antiferromagnets MnF_2 and MnO.

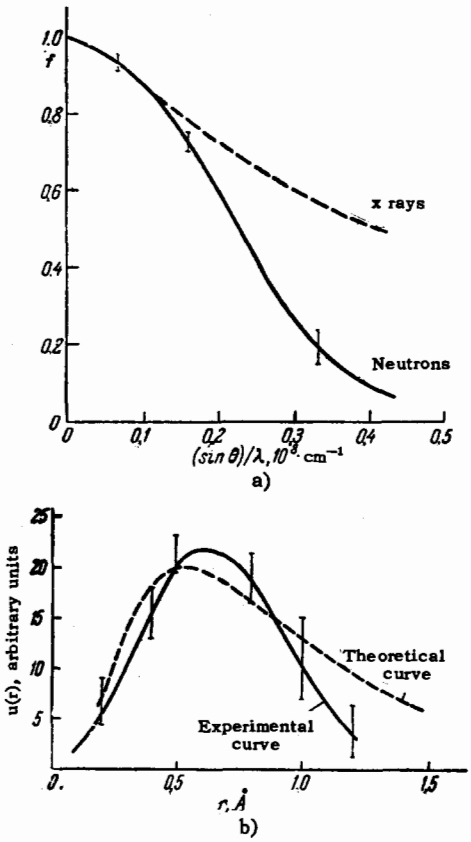

FIG. 3. a) Atomic factors: f_m – neutron (magnetic), f_a – x ray; b) radial distribution of magnetic electrons of 3d shell of Mn^{+2}.

unpolarized neutron beam we have in the mean $(\mathbf{q}\cdot\boldsymbol{\lambda}) = 0$, and we obtain from (4)

$$d\sigma = b^2 + p^2q^2. \qquad (9)$$

In this case the nuclear and magnetic scattering are incoherent and their intensities add up. To separate the two scattering components we can use diffraction in magnetized single crystals and control the magnetic interaction vector $\mathbf{q}$ by varying the direction of the magnetizing field $\mathbf{H}$. The most important two cases are:

a) field $\mathbf{H}$ and vector $\mathbf{K}$ parallel to ϵ,

b) field $\mathbf{H}$ and vector $\mathbf{K}$ perpendicular to ϵ.

In the former case $q = 0$ and consequently the reflection intensity is due only to nuclear scattering, while in the second case the total intensity is equal to the sum of the nuclear and magnetic scattering intensities. We can therefore determine the intensity and the ampl'tude of the magnetic part of the scattering.

Figure 4 shows the dependence of the intensity of the 111 reflection for a magnetite crystal on the intensity of the external magnetic field, the direction of which corresponds to cases a) and b). In the absence of the field the magnetic structure of the crystal breaks up into domains with axes aligned with the easy magnetization axes, parallel to those of [100].

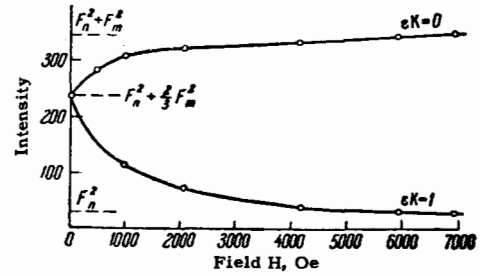

FIG. 4. Dependence of intensity of the 111 reflection of magnetite on the intensity of the magnetic field. F_n^2 – nuclear structure factor, F_m – magnetic structure factor.

In this case the mean value of q^2 is $\frac{2}{3}$. When an external field is applied, the intensity of the reflection depends on the direction of the field and on its magnitude, until saturation is reached. The difference between the curves at saturation characterizes the intensity of the magnetic scattering.

Production of polarized neutrons. A much more effective way of investigating magnetic structures is to use polarized neutrons, which can be produced by polarizing crystals, such as ferromagnetic or ferrimagnetic crystals that satisfy certain additional requirements. In accordance with the rules for space quantization, the spins of the neutrons passing through a magnetized single-domain crystal are oriented either parallel or antiparallel to the direction of the magnetic field. These two polarized beams, for which $(\mathbf{q}\cdot\boldsymbol{\lambda}) = \pm 1$, correspond to different effective scattering cross sections:

$$\sigma_+ = (b+p)^2,$$
$$\sigma_- = (b-p)^2. \qquad (10)$$

If the crystal contains a family of reflecting planes for which the nuclear and magnetic scattering amplitudes are approximately the same, $b \approx p$, then the reflected beam will contain neutrons with but one spin orientation. This condition is satisfied, for example, by the 220 reflection of a magnetite crystal (Fe_3O_4) and to an even greater degree by the 111 reflection of a crystal of cobalt-iron alloy, which has a high intensity and is not contaminated by the second-order reflection (at $\lambda/2$, where λ is the neutron wavelength). To eliminate the depolarizing influence of the domain structure and the incomplete orientation of the magnetic moments of the ferromagnet, the polarizer crystal is magnetized to saturation. Figure 5 shows how the degree of neutron polarization in a crystal of cobalt with 8% iron depends on the intensity of the applied magnetic field. The largest calculated degree of polarization is 99.1%.

Spectrograph for work with polarized neutrons. Figure 6 shows a double crystal spectrograph for obtaining polarized neutrons and for research with such neutrons.[3] The entire polarized neutron beam between the polarizing crystal and the inves-

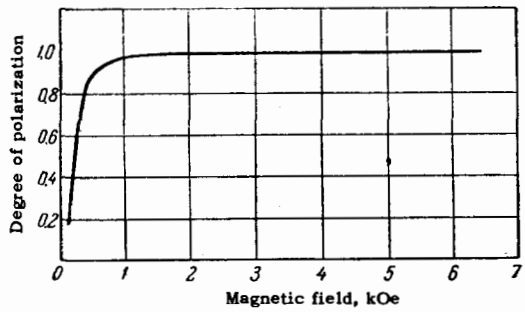

FIG. 5. Dependence of degree of polarization of neutrons by a Co+8% Fe crystal on the intensity of the magnetizing field.

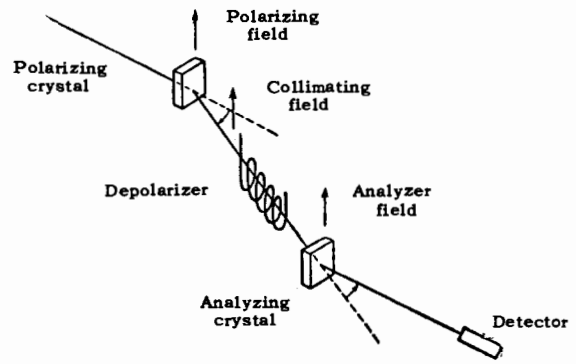

FIG. 6. Diagram showing neutron spectrograph for polarized neutrons.

tigated specimen, is situated in a magnetic collimator that maintains the polarization direction constant. This direction can be reversed if desired by means of a radio-frequency coil, in which the reversing field is turned on for a time that is short compared with the period of the Larmor precession.[4] The investigated crystal is magnetized by the external field parallel to the polarizing crystal. If necessary, a nonmagnetic iron plate approximately 0.5 mm thick is placed in the path of the neutrons to depolarize the beam.

The effectiveness of the method can be gauged from Fig. 7, which shows the change in intensity of the 111 reflection in a nickel crystal on going from parallel to antiparallel orientation. This change amounts to about 50%, whereas in work with unpolarized neutrons the fraction of magnetic scattering amounts to only 0.6% of the total intensity.

2. DETERMINATION OF ATOMIC MAGNETIC MOMENTS

Atomic magnetic moments can be determined from magnetic measurements. If the magnet contains several kinds of atoms, however, the magnetic data yield only the average atomic moments. A neutron-diffraction determination of the magnetic structure yields the magnetic moments of the individual atoms.

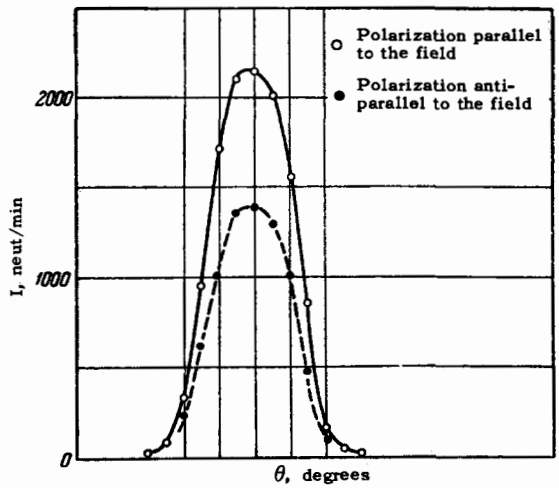

FIG. 7. Variation in intensity of the 111 reflection of a nickel crystal on changing the direction of neutron polarization.

If the magnetic structure is ordered, this can be done by measuring the intensity of the maxima of the magnetic coherent scattering. In measurements of partial magnetic moments of atomically and magnetically disordered compounds, the individual magnetic moments can be determined from the diffuse magnetic scattering, which in this case has the same nature as the isotopic or spin diffuse scattering.

Atomic magnetic moments in M_4N, where M is either Fe or Mn. In these nitrides the atoms of the metal form a cubic face-centered structure, with the cell centers occupied by nitrogen atoms (Fig. 8). Thus, Fe_4N can be regarded as the limiting composition of austenite nitride; the lattice period of the nitride is a = 3.795 Å and is greater than the lattice period of γ-Fe (a = 3.564 Å). Fe_4N is ferromagnetic with a Curie point T_C = 488°C; the magnetic moment per cell is about 9 μ_B, while the moment per iron atom is 2.25 μ_B, i.e., practically the same as for α-Fe. Several magnetic models were proposed to explain the magnetic properties of the iron nitride (Table I). In both models it is assumed that the atoms at the vertices of the cells have a configuration with the same number of valence electrons as for the free iron atom (but not for the metal). The difference between the models is that in the first the nitrogen atom is regarded as a donor, while in the second

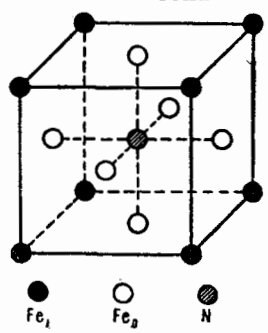

FIG. 8. Atomic structure of M_4N.

Table I. Magnetic models of Fe_4N

Atom	Coordinates	Wiener-Berger model[5]		Zener model[6]		Neutron diffraction
		Valence variations	μ	Valence variations	μ	μ
Fe_I	000	$3d^74s$	3	$3d^74s$	+3	2.98
Fe_{II}	$\frac{1}{2}\frac{1}{2}0, \frac{1}{2}0\frac{1}{2}, 0\frac{1}{2}\frac{1}{2}$	$3d^84s$	2	$3d^64s$	−4	2.01

it is regarded as an acceptor. The nitrogen atom, which has p^3 valence electrons, forms six octahedral bonds, directed towards the iron atoms located in the centers of the faces. These atoms have a moment equal to $2\mu_B$ in the first model and $4\mu_B$ in the second. In the first model the bond between the iron sublattices is assumed ferromagnetic, while in the second—antiferromagnetic, which leads to the same resultant moment, equal to $9\mu_B$. One can conceive also of a third model, similar to the first, in which all the iron atoms have the same average moment. For the first model one should observe magnetic superstructure lines, superimposed on the nitrogen nuclear scattering lines, whereas in the model with averaged moments there are no superstructure lines. To disclose the presence of weak superstructure lines with the aid of polarized neutrons, the difference between the intensities of the 100 and the 111 lines was established for a nitride single crystal with the applied magnetic field parallel to the scattering vector.[7] The change in intensity was found to be 3 and 14% respectively, thus confirming the correctness of the model with ordered arrangement of the moments. The antiferromagnetic model does not agree with the experimental intensities. The intensities of the magnetic superstructure lines were used to determine the moments of the iron atoms, namely $\mu_{Fe_I} = 2.98\mu_B$ and $\mu_{Fe_{II}} = 2.01\mu_B$, which corresponds quite well to the first model, in which the nitrogen atom behaves like a donor.

Wiener and Berger attempted to explain with the aid of the donor model the magnetic moments of the isomorphous compounds $NiFe_3N$, $PtFe_3N$, and Mn_4N. The extent to which such an explanation turns out to be deceptive was demonstrated by a neutron-diffraction investigation[8] of Mn_4N, which is chemically isomorphous with Fe_4N but which turns out to have a different magnetic structure. The magnetic moment per cell of manganese nitride is $1.2\mu_B$ and this compound is ferrimagnetic. Various magnetic models were proposed for this substance (Table II) with cubic configurational symmetry (the Guillaud model) and tetragonal models (Wiener-Berger, Juza-Puff), with different moment values. The cubic configuration of the magnetic structure was confirmed with the aid of polarized neutrons, but the values obtained for the moments differ greatly from those proposed by Guillaud. The moment of the Mn_I atoms not connected with nitrogen atoms in the cell corners, $3.5\mu_B$, is closer to the moment proposed by Juza and Puff for metallic manganese with electron configuration $3d^{6.8}4s^{0.2}$, which yields by Hund's rule a moment $3.2\mu_B$. The authors of [8] assume, following Bozorth, a manganese configuration $3d^{6.4}4s^{0.6}$ for the corner atoms, which yields by Hund's rule $3.6\mu_B$. The moment of the Mn_{II} atoms in the face centers cannot be obtained from Hund's rule for any reasonable electron configuration of manganese. Assuming that the nitrogen retains the donor functions in manganese nitride, as it does in iron nitride, we find that the manganese atoms bound to the nitrogen atoms "receive" from the latter one electron each, and have a configuration $3d^{7.4}4s^{0.6}$. The magnetic moment observed for these atoms holds for an electron distribution 3.3↑ and 4.1↓ between the subgroups with opposite spins, which contradicts the Hund rule. This unexpected result apparently agrees with the anomalous behavior of manganese in certain metallic phases and compounds, since a configuration $3d^64s$, with an electron distribution 4.2↑ and 1.8d↓, was proposed to explain the magnetic moment $2.4\mu_B$ of the manganese atoms, obtained by neutron diffraction in γ-Mn.[9]

Atomic magnetic moments of $FeNi_3$ and Fe_3Al. For $FeNi_3$, which has an ordered atomic structure, the contribution of the magnetic scattering to the superstructure line 100 and to the main lines, determined from the reduction in the intensity upon

Table II. Magnetic models of Mn_4N

Atom	Coordinates	Guillaud	Wiener-Berger	Juza-Puff	Neutron diffraction
Mn_I	000	+5	+4	+3.2	+3.5
Mn_{II}	$\frac{1}{2}\frac{1}{2}0, \frac{1}{2}0\frac{1}{2}, 0\frac{1}{2}\frac{1}{2}$	−2, −2, −2	+3, −3, −3	+2, −2, −2,	−0.7, −0.7, −0.7

application of a magnetic field in the direction of the scattering vector, yielded values $|\mu_{Ni-Fe}| = 2.11\mu_B$ and $\mu_{3/4Ni + 1/4Fe} = 1.21\mu_B$.[10] The latter value can also be determined from the magnetic saturation. An acceptable solution for these equations is $\mu_{Ni} = 0.67\mu_B$ and $\mu_{Fe} = 2.79\mu_B$. The former quantity is close to the atomic moment of pure nickel, whereas the second is much greater than the atomic moment in alpha-iron.

In the ordered alloy Fe_3Al, in which the corners of the cells are occupied by $8Fe_A$ while the centers are occupied by $4Al + 4Fe_D$, it was found with the aid of polarized neutrons[11] that the aluminum atoms, as expected, have no magnetic moment. The iron atoms in the D positions, surrounded by eight iron atoms, have a moment $\mu_{Fe_D} = 2.14\mu_B$, which is practically the same as in pure iron, whereas the iron atoms in the A positions, surrounded by four iron atoms and four aluminum atoms, have a much smaller moment, $\mu_{Fe_A} = 1.46\mu_B$. The moments of the iron sublattices are antiferromagnetically related. Consequently the average moment per iron atom is $1.68\mu_B$, which coincides with the magnetic data. The spins are directed parallel to the edge of the cube. The magnetic atomic factors coincide within two per cent for both types of iron atoms.

Atomic magnetic moments of transition metals. It is possible to separate in the neutron-diffraction pattern of alpha-iron the magnetic part of scattering, which is well described by formula (3), yielding for the resultant spin S = 1.11. This value coincides with the average magnetic moment for iron atom, $\mu_{Fe} = 2.22\mu_B$, obtained from the saturation magnetization. A similar agreement is obtained also for other ferromagnetic metals. Thus, the average magnetic moment in metallic cobalt is found by neutron diffraction to be $\mu_{Co} = 1.74\mu_B$, while magnetic measurements yield $1.71\mu_B$. Vanadium shows a neutron-diffraction pattern which seems unusual to the x-ray specialist (Fig. 9), where the 110 nuclear scattering maximum is hardly noticeable. This is due to the smallness of the nuclear scattering amplitude ($b_V = -0.05 \times 10^{-12}$ cm) and to the absence of the possible antiferromagnetic reflection 100. Nor is any background of paramagnetic scattering observed. We can thus conclude that $\mu_V < 0.1\mu_B$. There is more justification for calling vanadium atoms phantom atoms in neutron diffraction than hydrogen atoms in x-ray diffraction.

Magnetic moments in the paramagnetic region. The magnetic properties of the ferromagnetic metals Fe, Co, and Ni in the paramagnetic region above the Curie points are difficult to reconcile with their properties in the ferromagnetic region. High-temperature measurements of the magnetic susceptibility show that $1/\chi$ does not vary strictly linearly with temperature in the paramagnetic region for these metals, and consequently deviations from the Curie-Weiss law take place. Nevertheless, if we do use this law, the calculated atomic magnetic moments are found to be much greater in the paramagnetic region than in the ferromagnetic region. We thus obtain above the Curie point $3.4\mu_B$ for α-iron and even $10\mu_B$ for γ-iron, which is difficult to explain from the point of view of the electronic structure of the atoms of these metals. The magnetic measurements in the paramagnetic region may be greatly influenced by the short-range order in the arrangement of the magnetic moments, the theory of which was developed by S. V. Vonsovskiĭ.[39] The assumed short-range magnetic order was confirmed by neutron diffraction investigations.[36] The curves for the diffuse paramagnetic background for α-iron and for γ-iron differ little from each other. No jump is observed on going into the γ-domain for iron. The intensity of the diffuse background, calculated by means of formula (7) for the normal magnetic moment of the iron atom ($2.22\mu_B$), is even somewhat greater than the experimental values. A close-range magnetic order makes it difficult to determine exactly the magnetic moments from paramagnetic scattering, but it can be stated that the magnetic moments of α- and γ-iron can differ in the paramagnetic region from the atomic moment in the ferromagnetic region by not more than 25 per cent. The scattering of neutrons does not confirm the presence of large magnetic moments, as was assumed on the basis of measurements of the magnetic susceptibility of ferromagnets in the paramagnetic region.

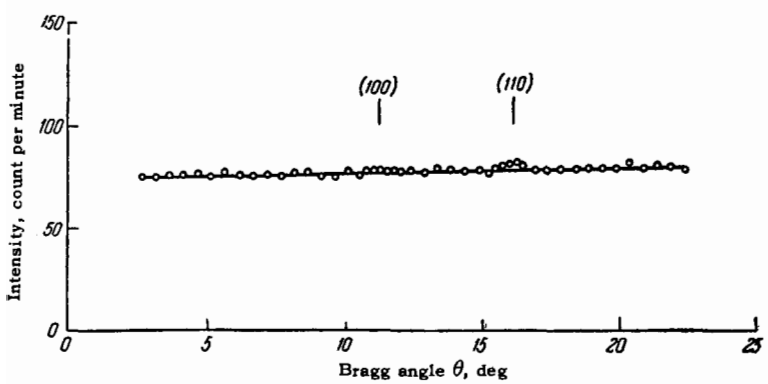

FIG. 9. Neutron diffraction pattern of vanadium.

3. MAGNETIC STRUCTURE OF TRANSITION METALS

Magnetic model of α-iron. From the agreement between the average atomic moments of the metals as obtained by neutron-diffraction and magnetic data in the ferromagnetic region, it would be incorrect to conclude that neutron diffraction makes no new contribution here. Neutron-diffraction investigations of transition metals do yield new data, which are essential for the understanding of their magnetic properties. Neutron diffraction has made it necessary to reject several magnetic models proposed to explain the observed average moments of metal atoms.

The following models of ordered magnetic structures were proposed for α-iron: 1) the corners of the cells are occupied by atoms with zero moments, and the centers of the cells by atoms with moments of $5\mu_B$,[12] corresponding to the moments of the Fe^{++} ion; 2) the corners and centers of the cells are occupied by atoms with moments $1\mu_B$ and $5\mu_B$, antiferromagnetically arranged.[6] The average moments given by these models, $2.5\mu_B$ and $2\mu_B$, differ noticeably from those obtained by experiment. An ordered arrangement of the spins is assumed in both models. The neutron-diffraction pattern should therefore disclose a magnetic-superstructure 100 line, but this was not observed in spite of a careful search. There is likewise no angle-dependent diffuse paramagnetic background, which should be observed if the spins have a random orientation (which is little likely for the ordered ferromagnetic state). Thus, neutron diffraction leads to an important result, since it shows that the fractional nature of the magnetic moments in ferromagnetic metal cannot be attributed to the presence of atoms with essentially different and fixed moments. The moments of all the iron atoms are the same, $2.22\mu_B$, this being due to the fast electronic transitions from one state to the other within a time ($\sim 10^{-16}$ sec) shorter than the time of passage of the neutron near the given atom ($\sim 10^{-13}$ sec).

Antiferromagnetic structures of transition metals. Depending on the sign of the exchange energy I in (8), the spin arrangement may be not only parallel, but also antiparallel. This leads to antiferromagnetic structures, such as observed in manganese and in chromium.

a) Manganese. In a neutron diffraction investigation of a Cu-Mn alloy,[9] an antiferromagnetic structure was found in γ-Mn, which has a tetragonal distorted face-centered atomic structure. In α-Mn, an antiferromagnetic structure is produced below $T_a = 100°K$, as evidenced by the appearance of peaks in the magnetic superstructure (Fig. 10a).[13] The intensity of the peaks decreases with temperature and follows a curve described by the Brillouin function (Fig. 10b). Paramagnetic scattering above T_a gives

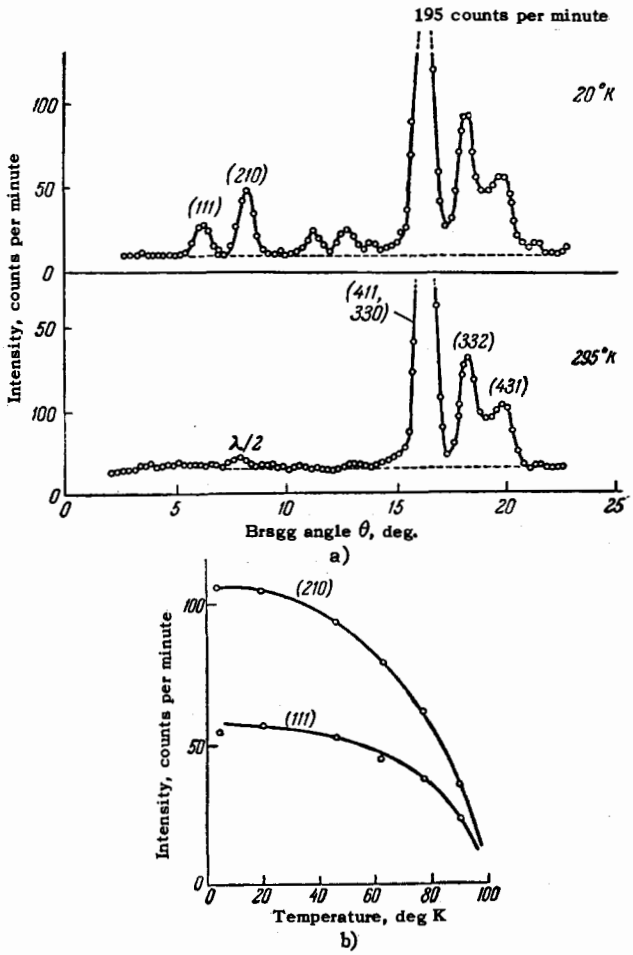

FIG. 10. a) Neutron diffraction pattern of α-Mn; b) temperature variation of the magnetic peak intensity.

for the average magnetic moment of manganese atoms a value $0.5\mu_B$.

An interpretation of the magnetic structure of α-Mn is very difficult because of the complexity of its atomic structure, which contains four types of structurally different manganese atoms and belongs to the space group $I\bar{4}3m-T_d^3$ without a symmetry center. A neutron-diffraction investigation has confirmed[14] the correctness of the earlier x-ray diffraction determination of the atomic structure (Bradley-Tzeulis, 1927), for which the distribution of the manganese atoms over the lattice complexes is shown in Table III. The coordination polyhedra about the atoms Mn_I and Mn_{II} are analogous to the polyhedra in Laves phases with composition AB_2; for Mn_{III} we have a 13-vertex polyhedron and for Mn_{IV} we have a distorted octahedron. The Mn_I atoms are surrounded by a regular tetrahedron of Mn_{II} atoms, at distances of 2.82 Å in antiparallel orientation. The Mn_{II} atoms are surrounded by a distorted tetrahedron of Mn_{II} atoms (2.82 Å spacing) in an antiparallel orientation and six Mn_I atoms. The three closer ones (2.49 Å) are antiparallel, while the three

Table III. Model of magnetic structure of α-Mn and magnetic moments of atoms

Space group $I\bar{4}3m-T_d^3$			Magnetic model		Magnetic moments	
Type	Complex	Coordinates	000	$\frac{1}{2}, \frac{1}{2}, \frac{1}{2}$	A	B
Mn_I	2a	000	$\frac{1}{2}\cdot 2a$	$\frac{1}{2}\cdot 2a$	1.54	2.50
Mn_{II}	8c	$x=0.317$	$\frac{1}{2}\cdot 8c$	$\frac{1}{2}\cdot 8c$	1.54	2.50
Mn_{III}	24g	$x=0.356$ $y=0.042$	$\frac{1}{2}\cdot 24$	$\frac{1}{2}\cdot 24$	3.80	1.70
Mn_{IV}	24g	$x=0.089$ $y=0.278$	Disordered			

farther ones (2.96 A) are parallel. The Mn_{III} atoms have two Mn_{II} neighbors (at 2.49 and 2.96 Å) with antiparallel and parallel orientations and six Mn_{III} neighbors (2.67 Å), of which four are antiparallel and two parallel. With the exception of the last two Mn_{III} neighbors, the proposed magnetic-structure model agrees with the general rule that the sign of the exchange energy, and consequently the character of the mutual orientation of the moments, changes with increasing distance between atoms. According to data by Forer,[15] the exchange energy of Mn in its alloys reverses sign at ~ 2.85 Å. For Mn_{IV} atoms it is impossible to choose a model with an ordered spin arrangement. This is apparently due to the fact that the nearest neighbors of the Mn_{IV} atoms are at very close distances (2.24—2.37 Å). The large Fermi energy does not contribute in this case to an ordering of the spins. The described magnetic-structure model is shown in Table III, which indicates two versions, A and B, of possible values of magnetic moments. The total number of magnetic moments per cell is found in this case to be large and greater than the moment estimated from the diffuse paramagnetic background at temperatures above T_a. To make more precise the magnetic structure of α-Mn and to determine the orientations of the moments relative to the axes, researches on single crystals are necessary.

The neutron-diffraction patterns of β-Mn are the same for 298 and 4.2°K, and in spite of a careful search, no antiferromagnetic structure maxima have been observed.[14] The paramagnetic scattering background does not decrease on cooling to helium temperatures, thus indicating that the paramagnetism is conserved. Research on single crystals is likewise desirable for this manganese modification.

b) Chromium. The temperature curves of many physical properties of chromium show more or less sharply pronounced anomalies in the vicinity of 40°C (Fig. 11). The electric resistivity (Fig. 11a) exhibits a certain increase on cooling, similar to the change in $\rho(T)$ for rare-earth metals in the anti-ferromagnetic transformation (cf. Fig. 37). The curve for the shear modulus (Fig. 11b) shows a small ledge, while the internal-friction curve (Fig. 11c) has a sharp minimum, which coincides in position with the minimum of the modulus of elasticity (Fig. 11d). The internal-friction curve has also a second small minimum at −152°C. Anomalies are also observed at 40°C in the thermal expansion (Fig. 11e) and in the thermal emf. The magnetic susceptibility curve (Fig. 11f) shows no singularities in this region,[16] if we disregard the general increase in χ with increasing temperature. The reason for the foregoing anomalies in chromium remained unexplained for a long time; an attempt was made to relate it to the impurities. Anomalies in the shear modulus and in the internal friction were observed near the antiferromagnetic transformation points for a whole series of substances. A possible explanation for these anomalies was recently proposed by D. A. Evtushenko and R. Z. Levitin.[109] A neutron-diffraction investigation of the magnetic structure of chromium has disclosed many interesting transformations of this structure, which apparently explain the foregoing anomalies, although one could hardly deduce from the form of the $\rho(T)$ curve that these anomalies were connected with just the magnetic transformations.

A neutron-diffraction investigation of polycrystalline chromium[13] was carried out to check Zener's theory, where it is assumed that although chromium displays no macroscopic magnetic properties, its atoms nonetheless have a large magnetic moment, $5\mu_B$, corresponding to five unpaired 3d electrons. In the metal these moments are antiferromagnetically arranged, and consequently the resultant moment is zero. At 20°K very weak maxima of the magnetic superstructure are observed, on the basis of which the magnetic moment per atom does not exceed $0.4\mu_B$. The paramagnetic background is also very small.

Significant results were obtained in a neutron-diffraction investigation of a single crystal of chromium,[17] in which magnetic reflections could be observed. The distinguishing feature of the antiferromagnetic picture of chromium lies in the appearance of triplets below ~ 40°C (Fig. 12a) instead of the single 100 reflection. The central component of the 100 interference represents a 200 reflection for the harmonic $\lambda/2$, while the extreme components represent a magnetic doublet, as confirmed by the temperature dependence of the line intensity of this doublet (Fig. 12b). The asymmetry of the intensity of the doublet components is due to the rapid decrease of the magnetic form factor. The temperatures of the magnetic transformations, determined by neutron-diffraction, coincide with the temperatures of the anomalies in the physical properties of chromium. The intensity of the magnetic maxima is the same along the three axes of the [100] cube. The splitting of the magnetic

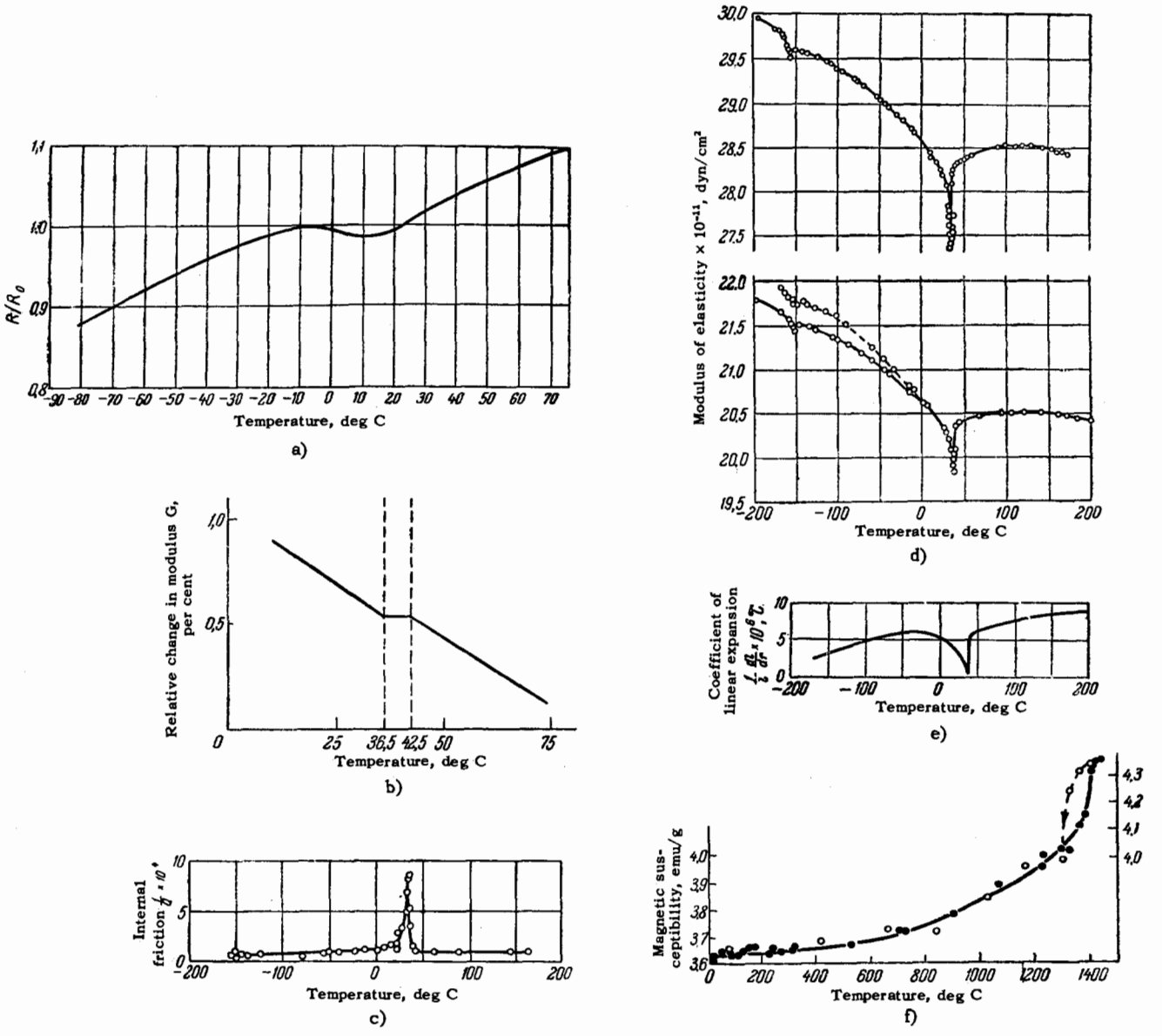

FIG. 11. Anomalies in the properties of chromium. a) Electric resistivity; b) shear modulus; c) internal friction; d) modulus of elasticity; e) thermal expansion; f) magnetic susceptibility.

doublet decreases somewhat with increasing temperature.

Neutron-diffraction data can be used to construct the reciprocal magnetic lattice of chromium (Fig. 13). Each site breaks up octahedrally into six components with an intensity distribution as shown in the figure. The splitting of the components along the coordinate axes is equal to $\frac{1}{39}$ Å^{-1} at room temperature, corresponding to approximately 14 chromium lattice periods. To explain this picture, an antiferromagnetic antiphase domain structure was proposed,[18,21] analogous to the antiphase domains in ordered CuAu alloys (Fig. 14).[19] Below the antiferromagnetic transformation temperature, the chromium crystals break up into domains with boundaries parallel to the faces of the cube. The edge of the true magnetic elementary cell is equal on the average to approximately 25 chemical cell lengths. The antiferromagnetic structure is formed in each domain because the spins of the chromium atoms in the centers and in the corners of the cells are antiparallel. Neighboring antiphase regions differ in that the spin is turned through 180°. The disordered arrangement of the spins in the crystal domains explains the observed intensity distribution of the magnetic superstructure maxima. The intensity of the magnetic maxima yields a magnetic moment of 0.47 μ_B per chromium atom, in agreement with the data of Shull and Wilkinson.[13] If the same magnetic form factor is assumed as for Mn^{++},[20] then the temperature dependence of I_{100} is described by a Brillouin function for $S = \frac{1}{2}$ and yields $T_a = 39°C$, which differs from $T_a = 175°C$ deter-

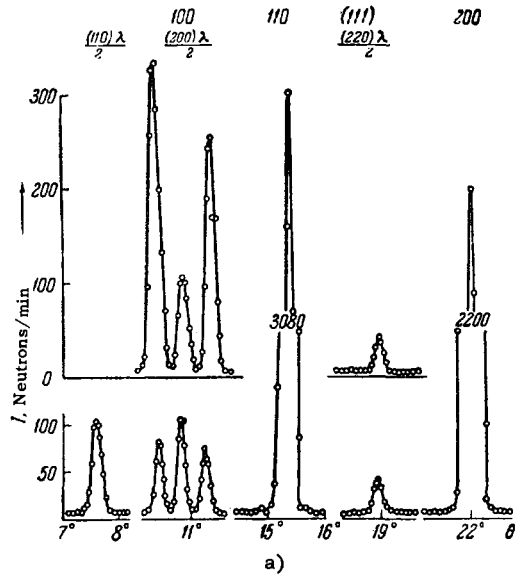

a)

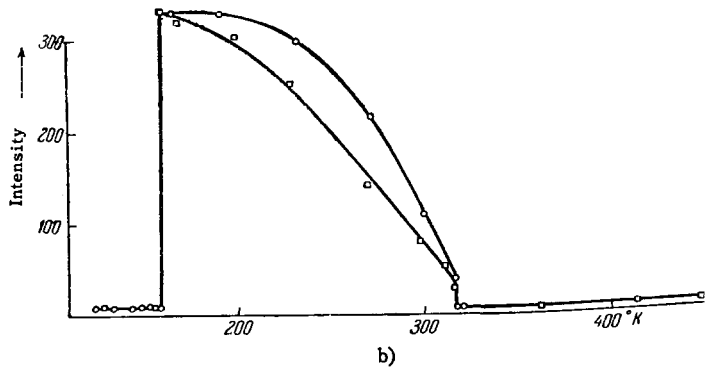

b)

FIG. 12. a) Magnetic doublets on neutron diffraction pattern of a single crystal of chromium. b) Temperature dependence of intensity of magnetic reflections in chromium. □ and ○ – on heating and cooling.

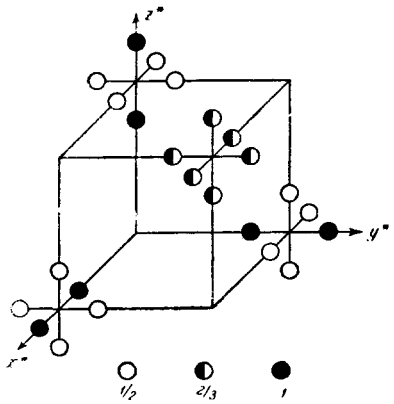

FIG. 13. Structure of reciprocal magnetic lattice sites of chromium.

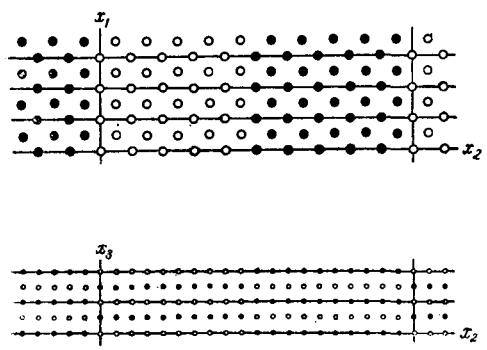

FIG. 14. Antiphase domains in CuAu.

mined by neutron diffraction for polycrystalline chromium.[13] The latter value for the temperature is also confirmed in [18].

Bacon[21] found that above T_a = 39°C the neutron-diffraction pattern of polycrystalline chromium retains a considerable "tail" of magnetic reflection, which can be traced in the temperature region up to 150—200°C. A weaker tail, which can be traced above 39°C, is observed in the single crystal. This indicates apparently that there are two antiferromagnetic transformation temperatures, one at 39°C and the other in the region of 200° C.

At −110°C a change is observed in the magnetic scattering pattern, consisting of the disappearance of the 0, 0, $^{24}/_{25}$ and 0, 0, $^{26}/_{25}$ reflections, in agreement with the data by Bykov and his co-workers, but the reflection 0, $^{1}/_{25}$, 1 is retained. Thus, the magnetic transformation at −110°C can be related to the change in the magnetic anisotropy. At room temperature the spins are parallel to the domain boundaries, while below −110°C they are perpendicular to the boundaries.[22]

Neutron diffraction discloses that, based on the magnetic reflections in chromium, there are apparently three magnetic transformations (Table IV), the temperatures of which are sensitive to weak effects

Table IV. Temperatures of magnetic transformations in chromium as obtained by neutron diffraction

Type of magnetic transformation	°C	°K
Change in magnetic anisotropy	−115	158
Change in antiferromagnetic structure	+35	308
?	+175	448

(impurity, strain), and for which various authors give slightly different values.

The first two transformations manifest themselves in the anomalies of the physical properties. The nature of the third transformation is still unclear. Bacon assumes that the last residues of the antiferromagnetic domain structure of chromium disappear at +175°C.

Bacon [21] also obtained some data on the influence of the grain size and certain impurities on the magnetic structure of chromium.

The chromium magnetic superstructure picture admits of another interpretation, based on the helical model. This hypothesis was advanced because calculation of the spin interaction energy with account of first and second neighbors has shown that a helical spin arrangement corresponds to a lower value of the energy. [23] However, the change in magnetic anisotropy in chromium, possible within the framework of the antiphase structure, does not agree with the helical model.

New class of magnetic structures—helical structures. The idea that nonlinear configurations are possible in addition to the parallel and antiparallel arrangement of the spins was soon confirmed. A helical magnetic structure was found [24] in $MnAu_2$, which has a tetragonal structure of the rutile type with layered arrangement of the atoms ... Au—Mn—Au—Mn—Au ... The magnetic moments of the manganese atoms lie in the planes of the layers and are parallel to each other within each layer. On going to the next layer, the moment direction rotates about the tetragonal axis by a constant angle φ. A helical structure manifests itself in neutron diffraction in practically the same manner as the antiphase domain structure. Each nuclear peak is accompanied by two magnetic reflections $(hkl)^+$ and $(hkl)^-$. The proposed helical model is in good agreement with the experimental intensities at $\varphi = 51°$ making the period of the magnetic superstructure along the atomic-structure axis equal to approximately seven interplanar distances.

A helical spin arrangement was also found in holmium, which has a hexagonal closed packed structure. The magnetic and thermal data imply two transformations in holmium, at 20.0 and 132°K. The low-temperature transformation is connected with the transition to the ferromagnetic state. Neutron diffraction has shown [25] that at 132°K a transition takes place from the paramagnetic state to the helical magnetic structure, with the helix axis parallel to the c axis. The irrational connection between the magnetic structure and the atomic structure can be seen from the fact that on going to each successive plane the spin rotation angle varies continuously from 48.8° at 119°K to 38.4° at 52°K. Thus, the magnetic helix in holmium untwists with decreasing temperature. The helical magnetic structure of holmium manifests itself in neutron diffraction by the fact that above 35°K a satellite pair, symmetrically arranged along the c axis, appears near each reciprocal lattice point. In particular, a very intense pair of magnetic reflections, connected with the origin (000), appears at small reflection angles.

The theory of neutron diffraction in helical structures was recently examined by Koehler, [26] who showed that equidistant magnetic satellites, lying along a reciprocal-lattice direction parallel to the helix axis, appear around the nuclear reflections. The possibility of occurrence of helical magnetic structures was considered theoretically in [27], and for tetragonal lattices in [28].

Description of magnetic symmetry. The symmetry of paramagnetic crystals is described, as is well known, by the ordinary (neutral) space groups. The symmetry of crystals with parallel and antiparallel moment orientations is described by black-white symmetry groups, proposed on the basis of the antisymmetry concept introduced by A. V. Shubnikov. [29] The total number of black-white space groups, including the uncolored space groups, as shown by Soviet crystallographers, [30] amounts to 1651. The discovery of helical magnetic structures incommensurate with the atomic lattice of the crystal complicates the problem of describing magnetic symmetry, since the magnetic symmetry group may not be connected directly with the atomic symmetry group. The complications that arise are point out [31] by one of the authors of the first work on the determination of magnetic symmetry of chalcopyrite. [32] It is possible that it will be necessary to use for this purpose the results of a study of the laws of color symmetry—spin rotation about the helical axis will correspond to a change in color.

Magnetic structures of vanadium and γ-iron. A jump in magnetic susceptibility is observed in vanadium at 250°K (Fig. 15), corresponding to a small kink on the electric-resistivity curve. The location of the jump depends on the impurities and drops by about 15° when 2% chromium or 3% cobalt are added. Neutron-diffraction [33] does not disclose any antiferromagnetism and confirms the conclusion [13] that the magnetic moment of vanadium is less than $0.1\mu_B$. Comparison with the data of [34] on dilute solid solutions shows that this anomaly of vanadium has nevertheless an antiferromagnetic nature.

Many authors have advanced the hypothesis that γ-iron is antiferromagnetic. [35] A neutron diffraction pattern of γ-iron, obtained at high temperature

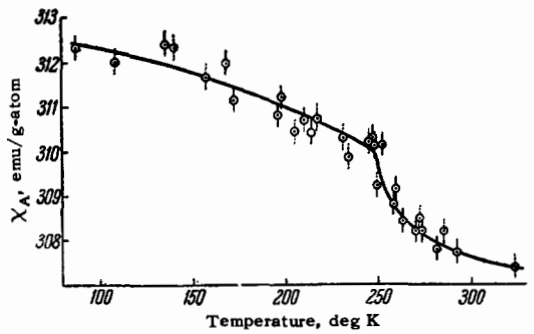

FIG. 15. Magnetic susceptibility curve for vanadium.

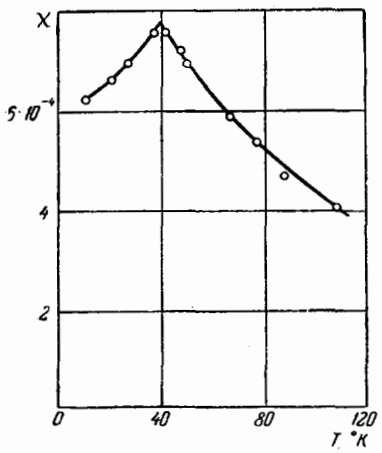

FIG. 16. Curve showing magnetic susceptibility for austenitic steel.

(971°C), i.e., in the equilibrium region of the gamma phase, does not show[36] any magnetic superstructure lines. An investigation of the magnetic properties of Fe–Mn alloys with face-centered cubic structure shows the presence of weak antiferromagnetism with a low antiferromagnetic transformation temperature. E. I. Kondorskiĭ and V. L. Sedov have observed in austenitic steel with 18% chromium and 9% nickel a clearly pronounced magnetic anomaly at 40°K (Fig. 16).[37] A neutron-diffraction investigation was made of the magnetic structure of this alloy at 10°K.[38] No magnetic superstructure lines were observed in this case, either. A possible way of explaining the discrepancies between the neutron-diffraction and magnetic data, as in the vanadium case considered above, is to assume that the fluctuation of the antiferromagnetism is fast compared with the time required to produce the neutron diffraction pattern.

4. MAGNETIC STRUCTURES OF CERTAIN COMPOUNDS

The survey[38a] gives the basic results of the first neutron-diffraction investigations of the magnetic structure of chemical compounds with an atomic structure of the type NaCl, α-Al_2O_3, spinel, and others. Since that time, much interesting work was done in this field. Owing to the lack of space, however, we shall discuss here the research done on compounds with other structures.

Perovskites of the iron group. An ideal structure of the perovskite type (Fig. 17a), or a structure of the ReO_3 type (Fig. 17b), is built around a cubic frame of ...B—O—B... linkages. The cations of smaller size, such as Mn^{+3}, Co^{+3}, Ti^{+4}, Mn^{+4}, and others are situated inside oxygen octahedra. The centers of the cells, which are free in the structure of the ReO_3 type, are occupied in the perovskite type structure by cations that are larger in dimension, such as La^{+3}, Nd^{+3}, Ca^{+2}, Sr^{+2}, Ba^{+2}, etc. In most cases the structures of these compounds are complicated by the presence of superstructures and symmetry distortions. These complications are connected with magnetic and dielectric (ferroelectric and antiferroelectric) phase transitions, frequently observed in these compounds. In compounds containing ions of transition metals, distortions may also be produced by the lifting of the d-level degeneracy. Compounds of the perovskite type, containing paramagnetic ions of transition and rare-earth metals, have ferromagnetic and antiferromagnetic properties.

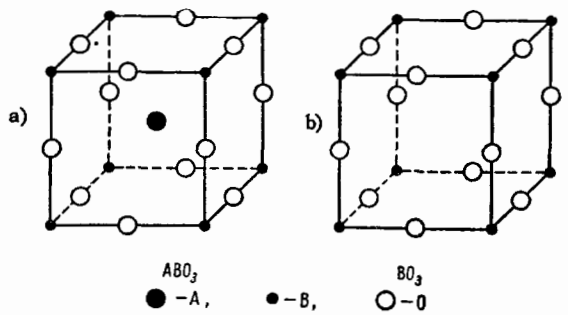

FIG. 17. Atomic structures: a) perovskite ABO_3, b) ReO_3.

One such compound is $LaMnO_3$ which can contain, depending on the conditions under which it was produced, up to 35% of tetravalent Mn^{+4} ions in addition to the trivalent Mn^{+3}. Manganese lanthanide has a monoclinically distorted cell[40] consisting of eight perovskite subcells. A similar structure is possessed by $CaMnO_3$, which forms with lanthanide a continuous series of solid solutions, in which the ratio of the trivalent to tetravalent manganese ions varies continuously. Neutron diffraction investigations of the system $(La_{1-x}Ca_x)MnO_3$ has disclosed[41] certain types of magnetic structures (Fig. 18, where only the manganese ions are shown). Manganese lanthanide $LaMnO_3$ has (Fig. 18a) a layered structure with a double period along the axis (type A). $CaMnO_3$ has a coordination structure similar to that of NaCl, with octahedra surrounding ions of opposite spins (type G). The periods are doubled along the three coordinate axes. The solid solution $(La_{0.2}Ca_{0.8})MnO_3$ has a chain structure (Fig. 18c)

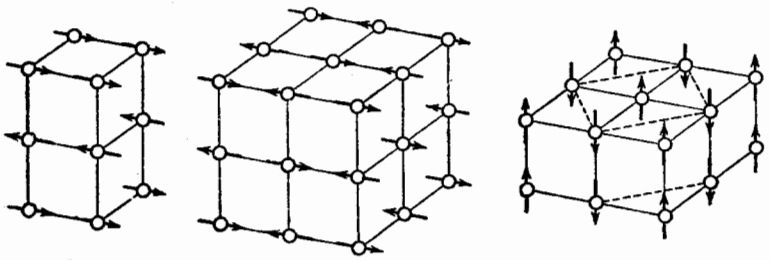

FIG. 18. Magnetic structures of $(La_{1-x}Ca_x)MnO_3$.

(type C). The periods are increased by $\sqrt{2}$ along the two coordinate axes. Solid solutions containing about 30% Mn^{+4} are ferromagnetic. In this case the magnetic cell coincides with the chemical cell (type B). These magnetic structures differ in the number of nearest neighbors with parallel (F) and antiparallel (A) spin orientations (Table V). For solid solutions with different concentrations, more complicated magnetic structures were observed, which can be reduced to combinations of the two simpler types.

Table V. Coordination relations of spins in octahedral magnetic structures

Type of magnetic structure	A	B	C	G
Number of neighbors F	6	4	2	0
Number of neighbors A	0	2	4	6

An analysis of the magnetic structure yields the following empirical rules for the spin orientations of neighboring manganese ions, which participate in the indirect exchange through the separating oxygen ions:

a) Mn^{+4}—O—Mn^{+4}—antiferromagnetic;

b) Mn^{+4}—O—Mn^{+3}—strongly ferromagnetic for $x < 0.5$;

c) Mn^{+3}—O—Mn^{+3}—ferromagnetic if Mn—Mn > 3.9 Å; antiferromagnetic if Mn—Mn < 3.9 Å.

For lanthanides of the transition metals, 42 analogous magnetic structures have been established (Table VI). There is a striking lack of isomorphism of magnetic structure for manganese lanthanide.

The antiferromagnetic transformation temperatures for isomorphous structures increase with increasing magnetic moment of the transition-metal atom. The solid solutions $La(Cr_xMn_{1-x})O_3$ were investigated by neutron diffraction in [43]. It was established that the regions where antiferromagnetic structures exist are asymmetrical with respect to the pure components: the magnetic structure of $LaCrO_3$ exists over a wide range of concentration, whereas the structure of $LaMnO_3$ is suppressed even by a small addition of chromium. At intermediate compositions, about 20% Cr^{+3}, ferromagnetism

Table VI. Magnetic structure of lanthanides of 3d-transition metals

Compound	$LaCrO_3$	$LaMnO_3$	$LaFeO_3$	$LaCoO_3$	$LaNiO_3$
Type of magnetic structure				No ordering	
Atomic magnetic moment μ_B	2,8	3,9	4,6		
T_a, °K	320	100	750		

was found of apparently ferrimagnetic origin, unlike the ferromagnetism of the $(La_{1-x}Ca_x)MnO_3$ system.

Perovskites of rare-earth metals. Interesting data were obtained in the investigation of rare-earth perovskites of the iron group ($MFeO_3$, where M = Nd, Ho, Er) containing two types of paramagnetic ions from different groups of the periodic table, with different values of exchange energy between them. According to x-ray data, they are isomorphous with $GdFeO_3$, which has a rhombic structure [44] with a cell consisting of four perovskite subcells. Neutron diffraction has disclosed in these compounds [45] two systems of magnetic moments (magnetic sublattices), they do not interact with each other (at least in the first approximation), and consequently each has its own Curie temperature.* At T_a values 760, 700, and 620°K for compounds of Nd, Ho, and Er respectively, the sublattices of the iron ions form the same antiferromagnetic type-G structure as in $LaFeO_3$. We consequently have here isomorphism of the magnetic structure for a large group of lanthanides. The moments of the Fe^{+3} ions in different compounds are approximately the same, namely 4.5_7, 4.6_0, and $4.6_2\,\mu_B$. At lower values of T_a, namely 6.5° and 4.3°K for $HoFeO_3$ and $EuFeO_3$ respectively, magnetic ordering of the sublattices of the rare-earth ions takes place. An antiferromagnetic chain structure of type C was established for $ErFeO_3$. The magnetic moment of Er^{+3} at 1.25°K is $5.8\,\mu_B$. A distorted antiferromagnetic structure was established for $HoFeO_3$, in which the spins in the (001) plane make a 27° angle with the [010] axis. This gives rise to a resultant magnetic moment directed along [100] and

*A similar picture, namely the existence of two independent magnetic sublattices, was observed by Bacon in Pt_3Fe.[116]

equal to 3.4 μ_B per formula unit. The magnetic moment of Ho^{+3} is 7.5 μ_B. A temperature dependence of the magnetic anisotropy was established. At room temperature the magnetic moment of the iron ions in $HoFeO_3$ and $ErFeO_3$ are parallel and antiparallel to the rhombic axis [100]. At 43°K the moments lie in the (100) plane. At 1.25°K the moments are parallel to [001] in $HoFeO_3$ and to [110] in $ErFeO_3$.

Antiferromagnetism of carbonates of the transition metals. The carbonates of the transition metals Mn, Co, Ni, and Fe have isomorphous crystal structures: they have a rhombohedral elementary cell with the metal atoms located at the corners and centers of the rhombohedra, and flat CO_3 groups perpendicular to the [111] axis. R. A. Alikhanov established [45a] that all these carbonates have an antiferromagnetic structure at low temperature. However, in spite of the atomic isomorphism, the magnetic structures of the four carbonates are different. This difference lies in the orientation of the magnetic moments in the lattice: if we denote by β the angle between the moment of the transition metal and the [111] direction, then the values of β are 0°, 46°, 63°, and 90° for the carbonates of iron, cobalt, nickel, and manganese, respectively. In addition, it has been established that the directions of the moments in $CoCO_3$ deviate from the symmetry plane in such a way that a weak ferromagnetism is observed. This weak ferromagnetism is consequently due to the violation of strict antiparallel alignment of the moments, and differs therefore from ferrimagnetism; a detailed thermodynamic analysis of this phenomenon was made by I. E. Dzyaloshinskii. [45b]

Trifluorides of the transition metals. Atomic structures of the compounds MF_3 can be described [46] on the basis of a ReO_3 structure close to the perovskite type. It is of interest to compare the magnetic structures of MF_3 with the structures of the corresponding perovskite compounds. The characteristics of the atomic structures of MF_3 are listed in Table VII.

MoF_3 and TaF_3 (Group I) have a cubic structure of the ReO_3 type. The fluorine atoms form a cubic close packing, with one-quarter of the sites occupied by the metal atoms. The remaining compounds, with the exception of MnF_3, have rhombohedral cells, containing two formula units each. Group II includes compounds in which the fluorine atoms form a hexagonal close packing. Group III contains compounds of 3d-metals having, like the compounds of group II, a rhombohedral structure, but intermediate between I and II. Differing from all these structural types is MnF_3, which has a monoclinically distorted cell with 12 formula units. [47] The MnF_6 octahedra are strongly distorted and it is possible to distinguish in them three pairs of non-equivalent Mn—F distances, short, medium, and long, equal to 1.8, 1.9, and 2.1 Å, respectively.

Table VII. Characteristics of atomic structure of MF_3

V (III)	Cr (III)	Mn (IV)	Fe (III)	Co (III)	Ni
Nb	Mo (I)	Te	Ru (II)	Rh (II)	Pd (II)
Ta (I)	W	Re	Os	Ir (II)	Pt

I — cubic, type ReO_3,
II — rhombohedral, type PdF_3,
III — rhombohedral, type VF_3,
IV — complex monoclinic, type MnF_3.

Neutron diffraction [48] has disclosed in most trifluorides of the iron group antiferromagnetic structures (Table VIII) that are analogous to the structures of the perovskite group (Table VI). These structures are isomorphous, again with the exception of the manganese compound. The values of the moments correspond to those of trivalent ions Cr^{+3} and Fe^{+3}. For cobalt, a moment somewhat greater than 4 μ_B was obtained, indicating apparently a contribution from the orbital moments.* The temperatures of the antiferromagnetic transformations of the perovskites and the trifluorides are in close correspondence.

The magnetic properties of the MF_3 compound for 4d and 5d transition metals differ greatly from those of the analogous compounds of the 3d metals. Magnetic susceptibility measurements show the magnetic moments of the 4d and 5d compounds to be very small compared with the moments of the iron-group trifluorides. An investigation of the magnetic structures is also of interest for a clarification of the electron configurations of the transition metal ions. MoF_3, RuF_3, and PdF_3 were investigated. [49] Neutron diffraction patterns taken for RuF_3 and PdF_3 at 298 and 4.2°K showed no magnetic ordering. Nor is there any angle-dependent diffuse paramagnetic scattering at room temperature. The magnetic moments of the ions Pd^{+3} and Ru^{+3} are therefore small, whereas by analogy with the corresponding metals of the 3d subgroup their moments should equal 3 μ_B and 5 μ_B. Two magnetic maxima are seen at 4.2°K, analogous to the maxima for CrF_3. The magnetic structures of these compounds are isomorphous and correspond to the G type. The directions of the moments are almost perpendicular to the trigonal axis. The temperature dependence of the intensity of the magnetic reflection is described by a Brillouin function and yields T_a = 185°K, whereas for CrF_3 we have T_a = 80°K. This shows that the magnetic bond in the 4d compounds is greater than the analogous 3d compound. The magnetic moment of the molyb-

*A considerable contribution of the orbital moment was similarly observed earlier in cobalt oxide (see [38e]).

Table VIII. Magnetic structure of trifluorides of 3d-metals

Compound	VF_3	CrF_3	MnF_3	FeF_3	CoF_3
Type of magnetic structure . .	no	*G*	*A*	*G*	*G*
Spin direction . .	—	$\perp c$	—	$\perp c$	$\parallel c$
Atomic magnetic moment μ_B	—	3	—	5	>4
T_a, °K	—	80	43	394	460

denum ion is found from the diffusion paramagnetic scattering to be $3\mu_B$.

Lifting of the degeneracy of the d-levels in the crystal field. In the absence of an external field, the energies of the remaining states of the d subgroups are the same. These states differ in the symmetry of the wave functions, and can be assigned to two subgroups. The electron density maxima of the d_{z^2} and $d_{x^2-y^2}$ states (subgroup e_g) lie along the coordinate axes (Fig. 19a), while for the d_{xy} (Fig. 19b), d_{yz}, and d_{zx} states (subgroup t_{2g}) they lie

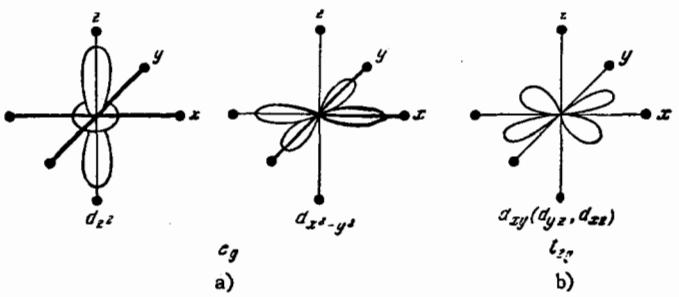

FIG. 19. Symmetry of d-states. • – cations.

along the bisectors of the coordinate angles. If the cation of the transition metal is octahedrally surrounded by six anions, the electrostatic repulsion of the electron clouds causes the energy of the t_{2g} levels to be lower than that of the e_g levels. Figure 20 shows the distribution of the energy levels for an ideal octahedral field (dashed) and for a tetragonal distorted field (for $c/a > 1$), in which further splitting into sublevels takes place. The level sequence may be different in a field of different symmetry. In a tetrahedral field, for example, the level of the t_2 subgroup drops and that of the e_g subgroup rises. This effect enables us to understand many structural features (distortion of cubic symmetry, inequality of interatomic distances), observed in certain compounds and the complex ions of

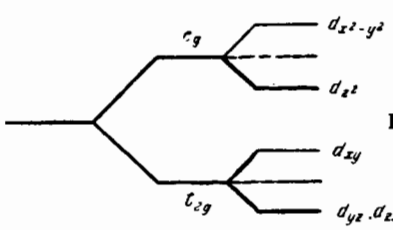

FIG. 20. Splitting of d-levels.

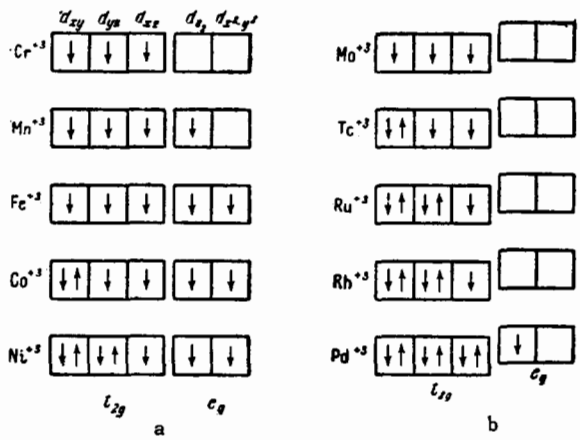

FIG. 21. Distribution of d-electrons over the e_g and t_{2g} levels in ions M^{+3} of transition metals: a) 3d groups, b) 4d groups.

transition metals.[50] Figure 21a shows the distribution of the d electrons over the t_{2g} and e_g subgroups. The Mn^{+3} ion is distinguished by an asymmetrical filling of the e_g level. This can explain many "anomalies" in compounds of trivalent manganese, particularly the occurrence of the complex MnF_3 structure.

In perovskite structures the t_{2g} orbits of the cation overlap the p orbits of the neighboring anions that participate in the indirect magnetic exchange. The mechanism of such an exchange was proposed by Kramers[51] and investigated by Anderson[52] and Pratt.[53] Most magnetic structures observed in perovskites are explained on the basis of the following rules for indirect exchange:

a) The exchange is antiferromagnetic if the half-filled orbits of two magnetic cations overlap through the p-orbits of the anion.

b) The exchange is antiferromagnetic if two empty orbits of magnetic cations overlap through the anion.

c) The exchange is ferromagnetic when the empty orbit of the magnetic cation overlaps the unfilled orbit of the second magnetic cation through the anion.

Exchange in compounds of iron and cobalt corresponds to case a). The octahedral symmetry of the e_g orbit brings about the observed symmetry of the antiferromagnetic structure of the G type. Exchange in chromium compounds corresponds to case b), which leads to the same antiferromagnetic configuration. The compounds of manganese MnF_3 and $LaMnO_3$

have a layered magnetic structure, which can be attributed to the presence of only one electron on the e_g orbit. Assume that this is an electron in the d_{z^2} state. The corresponding distribution of the electron density is shown in Fig. 22. If we take the half-filled $d_{x^2-y^2}$ state, we obtain a similar distribution. In both cases an antiferromagnetic exchange of type b) is produced between the layers, in which the free orbits of the cation overlap the p orbits of the anions separating them. Inside the layers, ferromagnetic exchange of type c) is produced. The proposed spatial distribution of the electron orbits explains the nonequivalence of the interatomic distances of MnF in the distorted MnF_6 octahedron, with three pairs of distances k = 1.8 Å, c = 1.9 Å, and d = 2.1 Å (see Fig. 22), as observed by x-ray diffraction.[47]

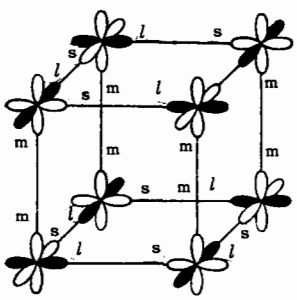

FIG. 22. Filling of the d orbits in MnF_3 (l – long, m – medium, s – short).

Violation of Hund's rule. The properties of the trifluorides of 4d metals can be explained qualitatively by assuming that Hund's rule does not hold here. The violation of this rule for ions of the higher series of transition metals was noted by Van Vleck[54] in an interpretation of data on paramagnetic susceptibility. This assumption agrees with the lifting of the degeneracy and the splitting of the 4d levels in complex transition metals.[55] As a result of this splitting (Fig. 21b) the lower lying t_{2g} cells are filled first with six electrons, and only then do the two e_g cells begin to be populated. In the Mo^{+3} ion there are only three 4d electrons, which occupy three t_{2g} cells, as is the case with Cr^{+3}. For the ions Pd^{+3} and Ru^{+3}, disregarding the lifting of the degeneracy and using Hund's rules, we should obtain, as in the case of free atoms, greater moments, 3 and 5 μ_B respectively, as for the ions Ni^{+3} and Fe^{+3} (Fig. 21a). With account of the described splitting, the magnetic moments of Pd^{+3} and Ru^{+3} are only equal to 1 μ_B. This is in qualitative agreement with the neutron-diffraction data. No magnetic ordering was observed in these compounds, this being possibly due to the small magnitude and rapid damping of the magnetic form factor. The accuracy with which the paramagnetic background is measured is insufficient to establish the presence of the small moment corresponding to S = ½. It is of interest to determine the magnetic moments of PdF_3 and RuF_3 from measurements of the paramagnetic susceptibility.

A phenomenological theory of magnetic exchange and of the magnetism of transition 3d metals, based on an examination of the splitting of the d levels in the crystal field and violation of the Hund rule, is developed in [56].

Magnetic anisotropy. Neutron diffraction has yielded many data on magnetic anisotropy. Some of these were mentioned earlier. One of the most recent investigations concerns the influence of small additions of chromium on the magnetic anisotropy of Mn_2Sb. Manganese antimonide has a tetragonal cell containing two weight particles. The four manganese atoms break up into two structurally and magnetically different groups, $2Mn_I$ and $Mn_{II} + Mn_{II}$ (Fig. 23a). The magnetic moments of Mn_I and Mn_{II} are respectively +2.13 and −3.87 μ_B.[57] Below +60°C,

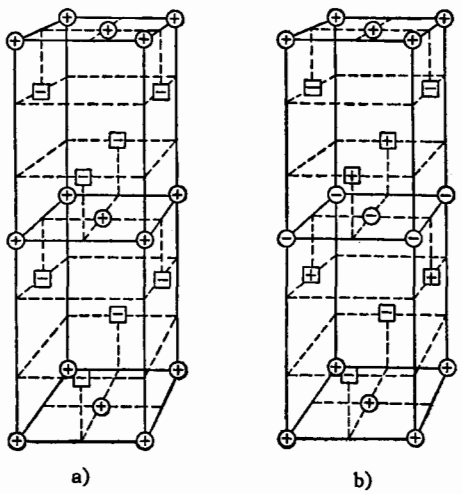

a) b)

FIG. 23. Magnetic structures: a) Mn_2Sb; b) Mn_2Sb with 2.3% Cr.

a ferrimagnetic structure is produced with antiparallel spins along the c axis. Between −20 and −40°C, the moments are oriented perpendicular to the c axis. A small addition of chromium produces, as indicated by magnetic data, an antiferromagnetic transformation (1 in Fig. 24), this being confirmed by neutron-diffraction data.[58] At +60°C, a magnetic structure similar to that of MnSb was found, while at −60°C the strong magnetic reflections 0, 0, ³/₂ and 0, 0, ⁵/₂ were observed, indicating a doubling of the period c of the magnetic cell. The sequence of spin orientation in the tetragonal layers $\cdots \overset{+}{\mathrm{I}}\ \overline{\mathrm{II}}\ \overline{\mathrm{II}}\ \overset{+}{\mathrm{I}} \cdots$ changes to $\cdots \overset{+}{\mathrm{I}}\ \overline{\mathrm{II}}\ \overset{+}{\mathrm{II}}\ \overline{\mathrm{I}}\ \overset{+}{\mathrm{II}}\ \overline{\mathrm{II}}\ \overset{+}{\mathrm{I}} \cdots$ corresponding to the antiferromagnetic structure (Fig. 23b). The transition from the ferromagnetic to the antiferromagnetic structure indicates a change in the sign of the exchange energy between the neighboring Mn_{II} layers. If Kittel's theory[59] concerning the phase transition from the ferromagnetic into the antiferromagnetic phase is valid in the present case, then the role of the chromium in the change of the magnetic properties of Mn_2Sb reduces to a decrease in the lattice

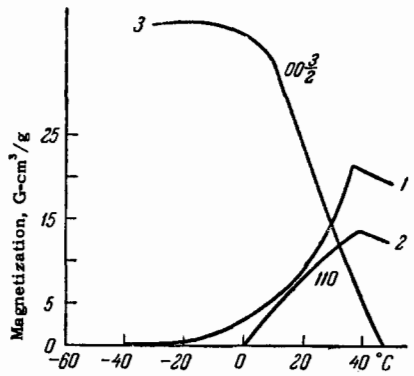

FIG. 24. Magnetization curve of $(Mn_{1.9}Cr_{0.1})(Sb_{0.95}In_{0.05})$ (1) and curve showing intensity of magnetic reflections 110 (2) and 0 0 3/2 (3) for Mn_2Sb with 2.3% Cr.

period. In the case of a chromium-containing compound the critical value of the period, at which the exchange energy reverses sign, occurs in the practically attainable region of thermal compression.

An analysis of the intensity of the principal magnetic reflection (110) (curve 2 of Fig. 24) and of the superstructure magnetic reflection 0, 0, $\frac{3}{2}$ (curve 3 of Fig. 24) establishes the magnetic anisotropy. Curve (2) is similar to the magnetization curve. The magnetic part of the 110 reflection is proportional to the saturation moment, which in turn is inversely proportional to the 0, 0, $\frac{3}{2}$ intensity. An investigation of the magnetic interaction vector $q^2 = \sin^2\alpha$ [Eq. (6)] shows that when the specimen is cooled below the point where the sign of the exchange reverses, the magnetic moments are rotated in the basal plane, whereas in Mn_2Sb such a rotation occurs only below −20°C. Thus, in Mn_2Sb with chromium the magnetic anisotropy in the antiferromagnetic region is negative (the moments are perpendicular to c), whereas the anisotropy of Mn_2Sb is positive in this temperature region. In the ferromagnetic region the anisotropy is the same in both substances.

5. MAGNETIC CRITICAL AND SMALL-ANGLE SCATTERING OF NEUTRONS

Critical scattering of neutrons. If long-wave neutrons which produce no Bragg reflections pass through a ferromagnet, an anomalous magnetic scattering is observed [60] with an intensity maximum at the Curie temperature (Fig. 25a). An investigation of magnetic scattering in magnetite [61] with short-wave neutrons ($\lambda < 2a$) has disclosed, in addition to the Bragg reflection 111, a superimposed diffuse reflection (Fig. 25b), the intensity of which reaches a maximum at a Curie temperature $T_C = 582$°C and is independent of the external magnetic field. These anomalous magnetic scattering effects are connected with fluctuations of the magnetization near the Curie point, in analogy with the critical opalescence of light near the ordinary critical temperature of the substance.

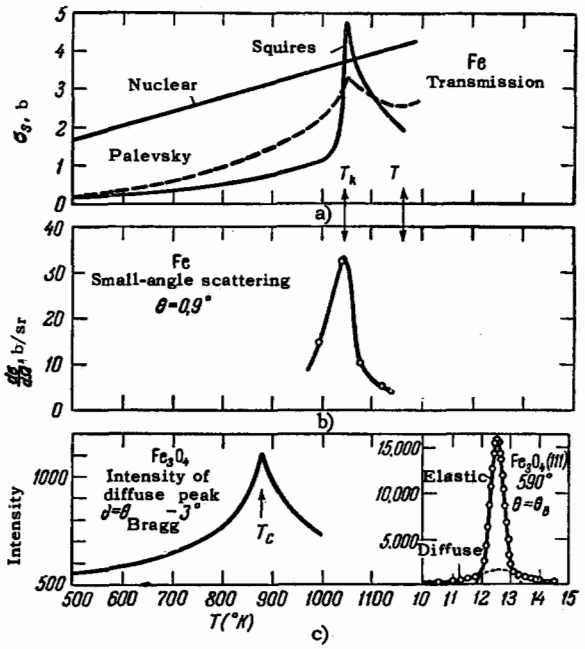

FIG. 25. Critical magnetic scattering in ferromagnets near T_C.

Generalized distribution function. Van Hove [62] generalized the Zernike-Prins [63] distribution function g(r) of a system of interacting particles by taking into account the correlations not only in space, but also in time, and introduced a function g(r,t). The function g(r) yields a scattering formula for solids, liquids, and gases, when the quantum state of the scattering system does not change and the energy exchange is negligibly small compared with the energy of the scattered particle. This corresponds to the scattering of x rays whose energy is large compared with the phonon energy. The space-time distribution function g(r,t) results in a general scattering formula, including cases when energy is transferred to the scattered particle. This is applicable to the scattering of cold and thermal neutrons, whose energies are either less than or comparable with the phonon energy. This formula, in particular, describes the scattering near the critical point in gases and liquids, and also the scattering in magnetic systems, connected with the loss of correlation in the spin arrangement and with large magnetization fluctuations near the Curie point. In this region, the theory predicts many critical scattering effects, such as the appearance of diffuse maxima near the magnetic Bragg reflections (Fig. 25c), the appearance of a considerable scattering in the small-angle region (Fig. 25b), and an increase in the total scattering cross section (Fig. 25a).

Van Hove's theory was developed in [64-65]. The last paper considers magnetization fluctuations and presents a theory of critical magnetic opalescence. The critical scattering was experimentally investigated in iron, [66] in Fe_3O_4, [67] where an analysis of the experimental results based on the de Gennes-

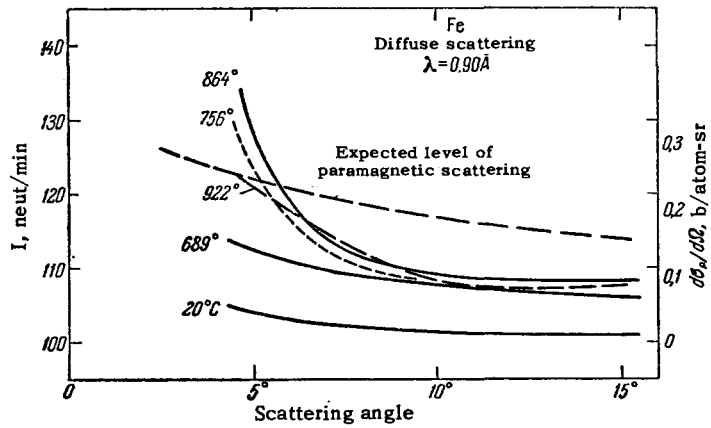

FIG. 26. Diffuse scattering of neutrons in iron at different temperatures.

Villain theory[65] is given, and in α-Fe_2O_3,[68] where it is shown that scattering on fluctuations in the critical region agrees with calculations based on the local form of the molecular field theory. Scattering of neutrons with account of time correlation was recently considered by Yu. A. Izyumov.[110]

Small-angle scattering. Great interest is attached to small-angle scattering of ferromagnets, observed by Wilkinson and Shull.[69] Figure 26 shows the considerable increase in small-angle scattering in α-iron on approaching the Curie point. This is similar to the scattering of x rays and light rays passing through a colloidal system, manifesting itself in the broadening of the primary beam and due to the density fluctuations in the medium. The angular width is inversely proportional to the average dimension of the system particles. Small-angle scattering in ferromagnets is connected with magnetization fluctuations near the Curie point and is essential for an understanding of the temperature variations of the spin-alignment regions. At 754°C the dimensions of the short-range spin order regions in iron lie, in accord with the small-angle neutron scattering data, range from 12 to 25 Å. Figure 27 shows the temperture dependence of the small-angle scattering, described by a curve with a well pronounced symmetrical maximum near T_C = 788°C. The vanishing of the short-range order, existing above T_C on going through the point of the polymorphous $\alpha \rightleftarrows \gamma$ transformation, is seen quite clearly.

Small-angle magnetic scattering is found also in nickel, where the small magnetic moment ($0.61\mu_B$) makes the scattering much less than in α-iron ($2.22\mu_B$). In magnetite Fe_3O_4 there are divalent and trivalent iron ions with large magnetic moments, $\pm 5\mu_B$ and $+4\mu_B$, whereas the average moment per iron ion is small, $4\mu_B/3$. The effect of small-angle scattering in magnetite is small. This shows that the intensity of the small-angle scattering is determined not by the moment of the individual atoms, but by the average moment, and consequently, the atomic groups retain the mutual orientation of the moments on going through the Curie point.

The magnitude of the diffuse scattering in iron at room temperature depends on the time exposed to higher temperatures. This dependence is not completely clear and may be connected with the temperature dependence of the magnetic refractive index.

Magnetic refraction of neutrons. The neutron refractive index in a ferromagnetic crystal is given by[70]

$$n^2 - 1 = -\frac{\lambda N a}{\pi} \pm \frac{\gamma B}{E}, \qquad (11)$$

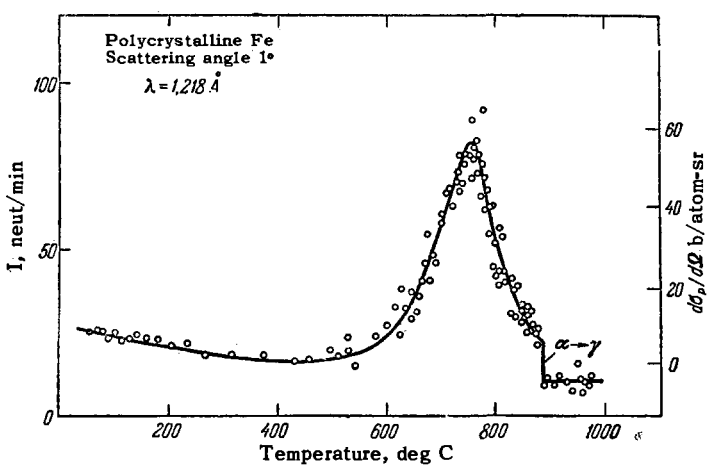

FIG. 27. Temperature dependence of intensity of small-angle scattering in iron.

where λ —neutron wavelength, N —number of nuclei per cm^3, a —nuclear radius, E —neutron energy, γ —the neutron magnetic moment, and B —magnetic saturation induction. The first term in the formula accounts for refraction due to scattering by the nuclei, and the second represents the magnetic part of the refractive index. The different signs correspond to two different neutron spin orientations relative to the magnetization vector. In scattering by differently oriented domains, refraction causes beam broadening. A temperature dependence was observed for the refractive index of magnetic scattering.[11] Since the domain structure depends on the heat treatment, this may cause in principle a change in the magnetic scattering pattern. Small-angle scattering in unmagnetized iron at room temperature, with a well collimated neutron beam (the entire effect amounted to 1′ on passing through 1 cm of iron) was first observed in [71]. This effect is attributed to multiple scattering on the domain boundaries, due to jumps in the magnetic refractive index. No beam broadening was observed in magnetized iron.

Certain characteristics of small-angle scattering. Small-angle scattering is the same in single-crystal and polycrystalline ferromagnets, and is independent of the dimensions and orientations of the crystal grains. Small-angle scattering is elastic, and although the energy of the incident neutrons, E = 0.100 eV, was somewhat greater in these experiments[69] than the exchange energy kT_C = 0.090 eV (as shown by investigations with a Sm_2O_3 filter with maximum capture cross section at neutron energy 0.100 eV), no changes in neutron energy greater than 5% were observed in small angle scattering. This indicates that scattering is not accompanied by energy exchange and is elastic in this case.

We note that whereas ferromagnetic short range order increases the paramagnetic scattering in the small-angle region[72] at the expense of scattering in other regions, antiferromagnetic order decreases the ferromagnetic scattering in the small-angle region (Fig. 1, curve for MnO). The antiferromagnetic domains in nickel oxide were studied by Roth,[73] who also investigated by neutron diffraction the effect that violations of stoichiometry of the iron oxide has on defects in the magnetic and crystal structures.[74]

Long-range and short-range magnetic orders. The Bragg magnetic maximum is determined by the long-range order in the spin alignment, which depends on the long-range magnetic dipole interaction. The energy of this interaction is comparable with the energy involved when a magnet is placed in an external magnetic field. Therefore the intensity of the selective magnetic maxima depends greatly on the external field intensity. This is caused by the fact that a sufficiently strong external field rotates the directions of domain magnetizations along the field, while the intensity of the magnetic scattering is determined by the mutual orientation of the magnetic moments and the scattering vector.

The diffuse magnetic maximum is determined by the short-range order, which depends on the short-range exchange interaction (8), the energy of which exceeds the energy of the magnet in an external magnetic field. Therefore the intensity of the diffuse peak does not depend on the external magnetic field. As shown in Fig. 28, a magnetic field of intensity H = 8000 Oe does not affect the intensity of the small-angle magnetic scattering at all. This scattering is the same in a single-domain state and in a magnetically disordered multi-domain state.

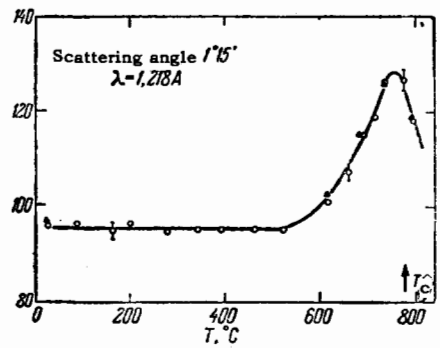

FIG. 28. Effect of external magnetic field on the intensity of small-angle scattering. o—nonmagnetized specimen; ▲—magnetized specimen.

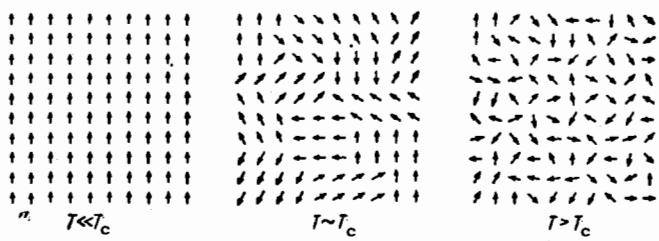

FIG. 29. Regions of spin correlation in magnetic lattice.

Dynamics of the spin-correlation regions. The short-range order changes rapidly as the Curie point is approached. The relaxation time of the magnetic fluctuations decreases on approaching T_C. A rough estimate[72] calls for the relaxation time to be $\sim 10^{-8}$ sec for temperatures different by 20° from T_C. Figure 29 shows schematically, in accord with the picture described above, the spin correlation regions in a magnetic lattice, both at temperatures much lower than T_C and near it, when long-range order exists, and at temperatures above T_C, when the regions of spin alignment correspond only to a short-range order. The spin correlation regions are dynamic in nature and are continuously displaced in the atomic structure.

6. NEUTRON SCATTERING BY SPIN WAVES

Spin waves. Magnons. The presence of exchange interactions leads to an ordering of the spins and to

the occurrence of a periodic magnetic structure of a space-lattice type, coinciding with the space lattice of the atomic structure in the case of ferromagnets, or representing a superstructure in the case of antiferromagnets. At low temperatures the magnetic lattice has a definite rigidity and although it is based on the atomic structure, it is independent to a considerable degree of the atomic lattice. Thus, for example, the magnetic lattice is transformed or destroyed on going through the magnetic-transformation points, whereas the atomic structure remains practically unchanged. Bloch [76,76a] has shown that destruction of the order in the spin lattice, for example a reversal in the direction of one spin, causes perturbations in the form of plane waves to propagate in the magnetic lattice with definite velocity. [77] These waves have been termed spin waves. They are analogous to elastic waves propagating in crystals.

Just as the elastic spectrum of a crystal can be regarded as consisting of elementary excitations or phonons, the spin-wave spectrum consists of elementary excitations called magnons. One can assign to the magnons a definite energy $E_m = h\nu$, an effective mass, and a momentum connected with the propagation vector κ. At low temperature the magnetic lattice is ordered. The scattering of particles capable of interacting with the magnetic lattice (neutrons or electrons) is then small. With increasing temperature and with increasing number and energy of the magnons, the scattering increases. For magnetic diffraction this means a decrease in the intensity of the selective magnetic maxima and an increase in the diffuse magnetic background. A theory of neutron scattering by spin waves was considered by G. Avakyants. [78] Scattering on magnons, just as scattering on photons, is described by the energy and momentum conservation laws

$$E - E' = \pm h\nu, \quad \mathbf{k} - \mathbf{k}' = 2\pi\tau \pm \varkappa + \omega, \tag{12}$$

where E and E′ are the energies of the incident and scattered neutrons, $\mathbf{k}$ and $\mathbf{k}'$ their momenta, τ the reciprocal lattice vector, and ω the basis vector for the complex lattices (for a simple lattice $\omega = 0$). The theory presupposes the existence of a relation between the spin-wave energy and its wave number (law of spin-wave dispersion).

Law of spin-wave dispersion. We can determine by experiment the energy and momenta of the scattered neutrons, and consequently the energy and the values of κ of a magnon interacting with a neutron. By repeating this operation we can determine the sought dispersion relation $\nu = \nu(\kappa)$.

Moorhouse [79] developed a spin-wave theory for ferromagnets and found a quadratic dispersion law. Elliot and Lowde [80] found a linear law for antiferromagnets. Equations (12) define in the reciprocal magnetic lattice space a surface which is the locus of the ends of the vectors $\mathbf{k}$. This surface is an ellipsoid in the case of scattering of slow neutrons by waves that obey the linear law

$$\nu = c\varkappa, \tag{13}$$

where the propagation velocity c of the spin perturbation is constant. [81] For ferromagnets the law is quadratic:

$$\nu = \alpha\left(\frac{h}{2m_0}\right)\varkappa^2. \tag{14}$$

In this case the scattering surface is a sphere. For ferromagnetic crystals, such as magnetite, the initial calculations of the spin waves gave different dispersion laws. A quadratic law was obtained in [82] and a linear one in [83], but the latter was inaccurately calculated. [84] A quadratic dispersion law was also obtained in [85,86]. Scattering of neutrons by magnons was recently considered by Maleev. [87]

It was assumed initially that spin-wave theory is valid only at low temperatures, to $\sim 0.1\,T_C$, for the spin waves interact with each other at higher temperatures. This means that the presence of irregularly oriented spins brings about the presence of irregularly oriented neighbors, for which the exchange energy is positive. Dyson has shown [88] that the interaction between magnons does not affect the validity of the theory. It is possible to use the spin-wave approximation over a sufficiently large temperature interval, as is the case for the spectrum of elastic waves in the anharmonic region.

Experiments with scattering on spin waves. The first confirmation of spin-wave theory was obtained by Brockhouse, [89] who investigated the spectrum of inelastic magnetic neutron scattering in a magnetic crystal, just as the phonon spectrum of vanadium [90] and aluminum crystals [91] was previously investigated by a similar method. The magnetite crystal is convenient because it has a high Curie temperature, $T_C = 850°K$, and the changes in the neutron energy upon scattering can be readily measured at room temperature. The experimental data are described by Eq. (12) and show the existence of wave-like spin perturbations. Figure 30 shows the magnon spectrum obtained in investigations of scattering near the 111 magnetic maximum of Fe_3O_4, wherein the deflection angle $\theta - \theta_0$ differed from the Bragg angle by amounts ranging from +20 to −40°, depending upon the angle of incidence. The spectrum obtained is of the acoustic type. In view of the large scatter of the experimental points, it is difficult to determine the dispersion law in this case. The figure shows curves corresponding to quadratic and linear dispersions. A linear spectrum would be correct for the phonon spectrum in the Debye approximation, while a sinusoidal law would be correct in the Born-

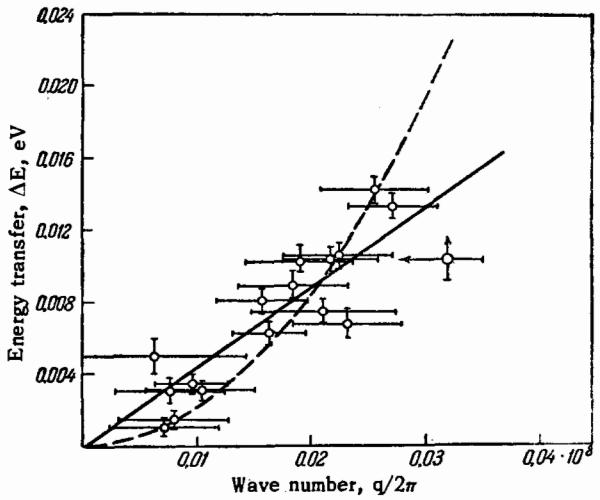

FIG. 30. Spectrum of magnons in Fe_3O_4.

Karman approximation. Judging from the slope of the curve in the initial region, the speed of propagation of the excitations, $c \sim 10^6$ cm/sec, is much higher than the speed of sound in magnetite, $c \sim 0.5 \times 10^5$ cm/sec.

It is shown in [89] that the experimental data are in best agreement with a quadratic law, for in this approximation a more likely value is obtained for the exchange energy in magnetite, $I_{AB} = -2 \times 10^{-3}$ eV, whereas the linear law gives about five times this value. Investigation[92] of inelastic scattering in magnetite has shown that the spin-wave theory is applicable over a wide temperature range. Figure 31 shows the temperature variations of the cross sections for iron atoms in magnetite. The linear portions of the curves correspond to regions where the spin-wave theory is applicable. The strong increase near the Curie temperature is due to the critical magnetic scattering, which cannot be described with the aid of spin waves. Measurement of the width of the magnetic 111 peak at an initial disorientation $\theta - \theta_0 = 9°$ shows (Fig. 32) that the spin-wave description

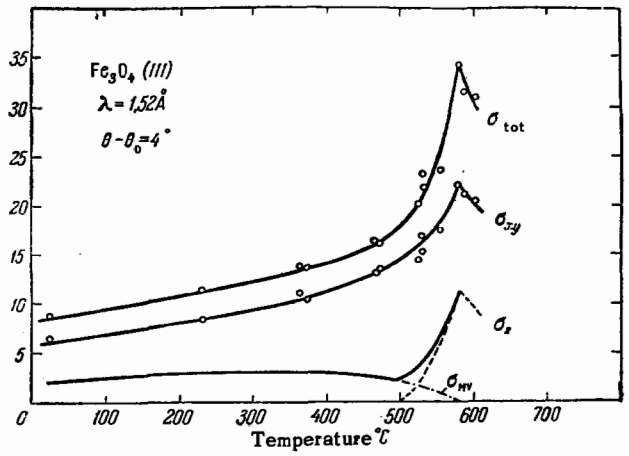

FIG. 31. Temperature dependence of total scattering cross section at $\theta - \theta_0 = 4°$. Linear regions correspond to scattering on spin waves.

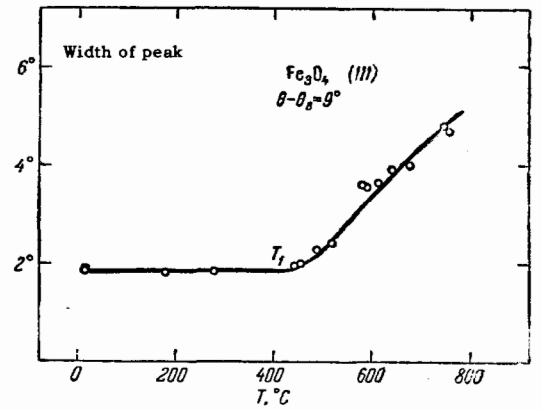

FIG. 32. Variation in width of magnetic maximum with temperature (at disorientation angle $\theta - \theta_0 = 9°$).

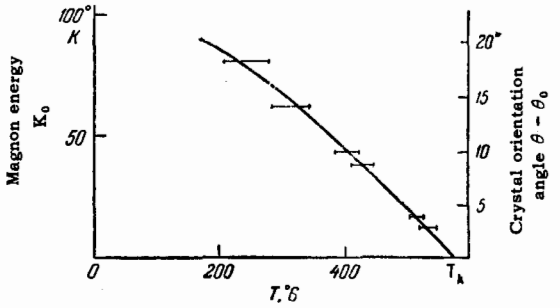

FIG. 33. Dependence of the temperature T_1 at which the spin-wave theory is valid on the magnon energy.

is valid up to a maximum temperature T_1. This temperature, as can be seen from Fig. 33, increases with decreasing magnon energy, in agreement with Dyson's findings that the interaction decreases for long waves. For very low magnon energies $E/k \sim 20°K$ the spin-wave picture is true up to $T_1 = 0.9\,T_C$. The proportionality of the cross section to the temperature in the case of low-energy magnons shows that they obey

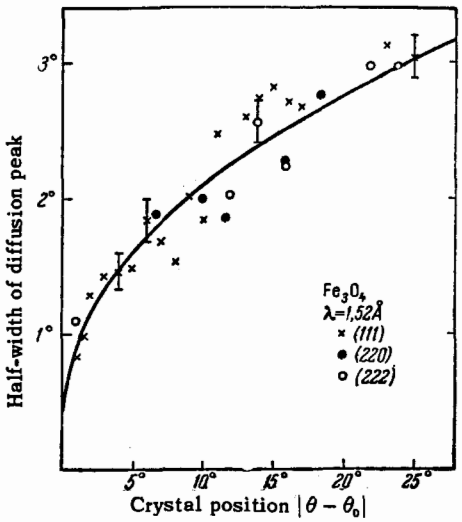

FIG. 34. Half-width of diffuse magnetic maxima as function of the angle $\theta - \theta_0$. Continuous curve – theoretical for a quadratic dispersion law.

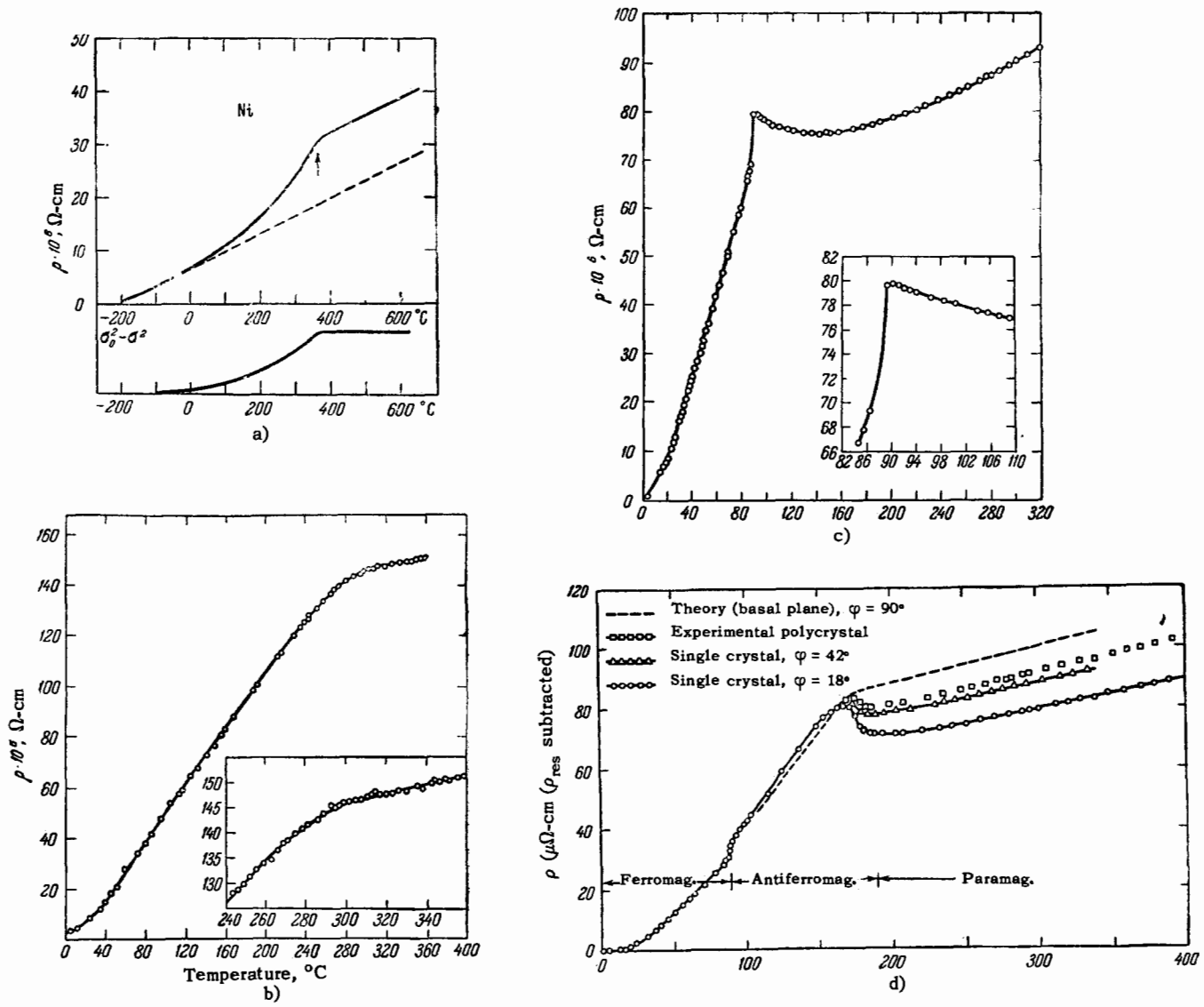

FIG. 35. Temperature dependence of electric resistivity of a) nickel, b) gadolinium, c) europium, d) dysprosium.

Bose-Einstein statistics. The experimental data confirm the quadratic dispersion law (Fig. 34) convincingly. The continuous curve is the theoretical relation resulting from assuming a quadratic dispersion.

Modifications of the results of [61] and [69], given in [92], show the effect of an external magnetic field on the intensity of inelastic magnetic scattering.

An investigation of neutron scattering in a single crystal of cobalt alloyed with 8% iron, which has a face-centered cubic lattice,[93] also confirms the correctness of the dispersion law in accord with the Bloch-Heisenberg wave theory. Certain spin waves have lifetimes $\sim 3 \times 10^{-13}$ sec.

For the antiferromagnetic hematite crystal α-Fe_2O_3, a linear dispersion law was obtained in accordance with the theory[68] and the magnon propagation speed was found to be 3.8×10^6 cm/sec = 38 km/sec, which is approximately ten times the phonon velocity. The value of the exchange energy is $I = -3.5 \times 10^{-3}$ eV. General dispersion relations were recently considered in [94], where a biquadratic relation was obtained. A dispersion law that holds for spin and electromagnetic waves was derived by M. A. Ginzburg.[111] The applicability of the spin-wave theory to antiferromagnets was demonstrated in [65].

7. MAGNETIC SCATTERING OF CONDUCTION ELECTRONS

Just as atomic ordering exerts an appreciable effect on the physical properties of crystalline bodies, so does magnetic ordering manifest itself in many respects, particularly in an additional resistance to conduction electrons.

Electric resistivity of disordered magnetic structure. Figure 35a shows the dependence of the electric resistivity of nickel on the temperature,[95] in-

dicating the presence of considerable additional resistivity above the Curie point, due to the disorder in the magnetic structure. A similar form is assumed by the electric resistivity curve of iron.[96,97] This effect, amounting to $\rho_{mag} = 4\,\mu\Omega$-cm in nickel, exceeds the effect $\rho_{at} = 3\,\mu\Omega$-cm in Cu_3Au, due to the disorder in the atomic structure. Both effects can be compared in a single alloy, AuMn, in which the spin disorder temperature is 65°C and the temperature at which the atomic structure of the solid solution becomes disordered is 627°C. In this alloy the magnetic disorder increases the electric resistivity five times more than the atomic disorder.

The influence of disturbances to the magnetic structure is particularly strong in rare-earth metals and their alloys, owing to the large atomic magnetic moment. Figure 35b shows a plot of $\rho = \rho(T)$ for gadolinium.[98] Figure 35c shows a similar curve for europium,[99] which has an antiferromagnetic transformation. The antiferromagnetic transition is accompanied by a certain increase in ρ. A similar effect occurs also in the antiferromagnetic transition in chromium (Fig. 11a). The irregular shape of the electric resistivity curve of dysprosium (Fig. 35d)[100] is due to the transition that takes place at $T_C = 90°K$ from the ferromagnetic into the antiferromagnetic state and the transition at $T_a = 175°K$ into a paramagnetic state, in which the electric resistivity varies linearily.

In crystals containing atoms or ions with unfilled electron shells and with spin moments S, additional scattering of the conduction electrons on the imperfections of the magnetic structure is produced. The total electric resistivity of such a crystal can be represented in the following form[101,102]

$$\varrho = \varrho_{res} + \varrho_{phon} + \varrho_{mag} \qquad (15)$$

comprising the residual, phonon, and magnon resistivities. Andersen and Legvold[103] determined the magnon part of the electric resistivity for the second half of the lanthanide group by extrapolating the resistivity in the paramagnetic region to 0°K, subtracting ρ_{res}, and introducing corrections ρ_{cor} using the Gruneisen temperature dependence of an ideal conductor. The magnetic scattering of the electrons resulting from the spin interaction is described in [104] by a formula similar to that for magnetic scattering of neutrons. For the paramagnetic region, a formula similar to (1) is valid. In Fig. 36, ρ_{mag} is plotted against $S(S+1)$. The experimental points are in good agreement with the linear relationship. Metals with large S have large values of ρ_{res}. The exchange interaction of the conduction electrons with the spins of the magnetic cores is an important factor deciding the scattering of the conduction electrons. We note that ρ_{mag} is not dependent, as might be expected, on the total magnetic moment vector or gI. This agrees with the fact that the

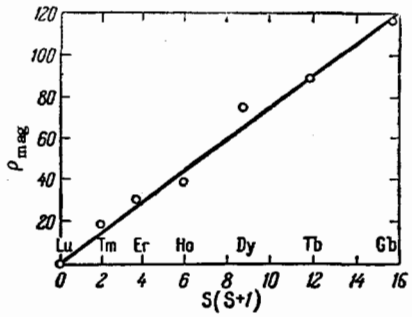

FIG. 36. Dependence of magnon scattering on S(S + 1).

Curie temperatures of the lanthanides, as noted by Néel,[105] follows a relation that results from the assumption that only the spins interact. Exchange interaction between conduction electrons and magnetic-ion spins can lead to an effective interaction between the spins of magnetic ions.[106]

A theory of electric resistivity in certain magnetic metals, which likewise includes an analogy with magnetic scattering of neutrons, was presented by deGennes and Friedel.[107] The scattering of conduction electrons by spin waves in ferromagnets was considered by Sh. Sh. Abel'skiĭ and E. A. Turov,[112] while similar scattering in antiferromagnets was considered by A. A. Berdyshev and I. N. Vlasov.[113] A spin mechanism of recombination of current carriers in ferromagnetic semiconductors was suggested by V. L. Bonch-Bruevich.

Spin interaction and superconductivity. It was shown experimentally[108] that in alloys of lanthanum with rare earths the suppression of superconductivity is determined by the spins of the dissolved atoms (Fig. 37). The authors of [103] have introduced in the microscopic theory of superconductivity a hypothetical additional electron-electron interaction between the conduction electrons, due to the exchange interaction with the magnons and based on the empirical equation

$$N(0)v = [N(0)v] - a\delta[S(S+1)]^2, \qquad (16)$$

where N(0) —energy density of electrons with like spin, v —average strength of the electron-electron interaction, a —concentration of magnetic rare-earth metal, and S —spin quantum number for the 4f electrons of the dissolved atoms. This made it possible to explain the variation of T_C in solid solutions of lanthanum with rare earths as a function of

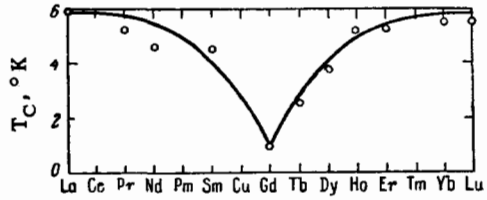

FIG. 37. Dependence of temperature transition into the superconducting state of lanthanum on the atomic number of one percent impurity of a rare-earth metal.

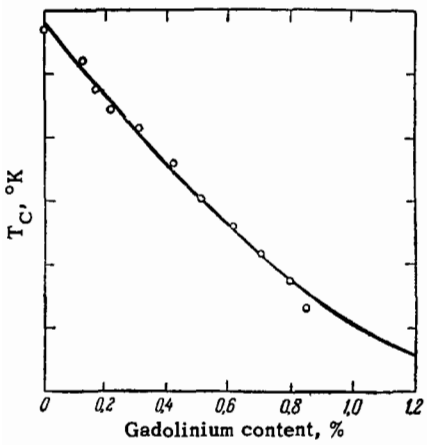

FIG. 38. Dependence of T_C of the superconductivity of a solid solution of La–Gd.

S (Fig. 37) and of the concentration a (Fig. 38). The effect of scattering of conduction electrons by spin waves of a ferromagnet on the temperature of transition to the superconducting state was considered by B. V. Karpenko.[115]

* * *

Magnetic neutron diffraction is rapidly developing and is being used to investigate an increasing variety of substances. The investigation of magnetic structure has yielded principally new results which are of great significance for the determination of the electron structure of matter, the development of solid state theory, and important practical applications.

[1] G. E. Bacon, Neutron Diffraction, Oxford University Press, 1957.
[2] R. Halpern and M. H. Johnson, Phys. Rev. **55**, 898 (1939).
[3] Nathans, Shull, Shirane, and Andersen, J. Phys. Chem. Solids **10**, 136 (1959).
[4] Burgy, Hughes, Wallace, Heller, and Woolf, Phys. Rev. **80**, 953 (1950).
[5] G. W. Wiener and T. A. Berger, J. Metals **7**, 360 (1955).
[6] C. Zener, Phys. Rev. **85**, 324 (1952).
[7] B. C. Frazer, Phys. Rev. **112**, 751 (1958).
[8] Takei, Shirane, and Frazer, Phys. Rev. **119**, 127 (1960).
[9] Bacon, Dunmur, Smith, and Strert, Proc. Roy. Soc. **A241**, 223 (1957).
[10] M. K. Wilkinson and C. G. Shull, Phys. Rev. **90**, 374 (1953).
[11] Nathans, Pigott, and Shull, J. Phys. Chem. Solids **6**, 38 (1958).
[12] Hume-Rothery, Irving, and Williams, Proc. Roy. Soc. **A208**, 431 (1951).
[13] C. G. Shull and M. K. Wilkinson, Revs. Modern Phys. **25**, 100 (1953).
[14] J. S. Kasper and B. W. Roberts, Phys. Rev. **101**, 537 (1956).
[15] R. Forer, Ann. Phys. (12) **7**, 605 (1952).
[16] A. H. Sully, Chromium (Russ. trans.), Moscow, Metallurgizdat, 1959.
[17] Bykov, Golovkin, Ageev, Levdik, and Vinogradov, DAN SSSR, **128**, 1153 (1959), Soviet Phys. Doklady **4**, 1070 (1960).
[18] Corliss, Elliot, and Hastings, Phys. Rev. Lett. **3**, 211 (1959).
[19] C. H. Johansen and J. O. Linde, Ann. Phys. **25**, 1 (1936).
[20] Corliss, Elliot, and Hastings, Phys. Rev. **104**, 924 (1956).
[21] G. E. Bacon, Bull. Amer. Phys. Soc. (BAPS) **5**, 455 (1960); Acta Crystallogr. **14**, 823 (1961).
[22] J. M. Hastings, BAPS **5**, 455 (1960).
[23] T. A. Kaplan, Phys. Rev. **116**, 888 (1959); B. R. Cooper, Phys. Rev. **118**, 135 (1960).
[24] Herpin, Meriel, and Villain, Compt. rend. **249**, 1334 (1959).
[25] Koehler, Cable, Wollan, and Wilkinson, BAPS **5**, 459 (1960).
[26] W. C. Koehler, Acta Crystallogr. **14**, 535 (1961).
[27] J. Villain, J. Phys. Chem. Solids **11**, 303 (1959).
[28] A. Yoshimori, J. Phys. Soc. Japan **14**, 807 (1959).
[29] G. S. Zhdanov, Fizika tverdogo tela (Solid State Physics), MGU, 1961, p. 152.
[30] A. M. Zamorzaev, Dissertation (Leningrad 1953); Belov, Neronova, and Smirnova, Trudy (Works) Institute of Crystallography, **11**, 33 (1955).
[31] J. D. H. Donney, BAPS **5**, 455 (1960).
[32] Donney, Donney, Elliot, and Hastings, Phys. Rev. **112**, 1917 (1958).
[33] J. P. Burger and M. A. Taylor, Phys. Rev. Lett. **6**, 185 (1961).
[34] G. de Vreis, J. phys. et radium **20**, 438 (1959).
[35] F. Bader, Z. Naturforsch. **8a**, 675 (1953).
[36] M. K. Wilkinson and C. G. Shull, Phys. Rev. **103**, 516 (1956).
[37] E. I. Kondorskii and V. I. Sedov, JETP **35**, 1579 (1958), Soviet Phys. JETP **8**, 1104 (1959).
[38] Zhdanov, Ozerov, and Kiselev, Kristallografiya **7** (1962), in press; Soviet Phys. Crystallography **7**, in press.
[38a] R. P. Ozerov, UFN **47**, 445 (1952).
[39] S. V. Vonsovskii, DAN SSSR **27**, 650 (1940).
[40] H. L. Yakel, Acta Crystallogr. **8**, 394 (1955).
[41] E. O. Wollan and W. C. Koehler, Phys. Rev. **100**, 545 (1955).
[42] W. C. Koehler and E. O. Wollan, J. Phys. Chem. Solids **2**, 100 (1957).
[43] U. H. Bents, Phys. Rev. **106**, 387 (1957).
[44] S. Geller, J. Chem. Phys. **24**, 1236 (1956).
[45] Koehler, Wollan, and Wilkinson, Phys. Rev. **118**, 58 (1960).
[45a] R. A. Alikhanov, JETP **36**, 1690 (1959) and **39**, 1481 (1960); Soviet Phys. JETP **9**, 1204 (1959) and **12**, 1028 (1961); Conference on Ferro and Antiferromagnetism (Leningrad, May, 1961), Abstracts, p. 8.

[45b] I. E. Dzyaloshinskii, JETP **32**, 1547 (1957), Soviet Phys. JETP **5**, 1259 (1957).
[46] Hepworth, Jack, Peacock, and Westland, Acta Crystallogr. **10**, 63 (1957).
[47] M. A. Hepworth and K. H. Jack, Acta Crystallogr. **10**, 345 (1957).
[48] Wollan, Child, Koehler, and Wilkinson, Phys. Rev. **112**, 1132 (1958).
[49] Wilkinson, Wollan, Child, and Cable, Phys. Rev. **121**, 74 (1961).
[50] J. D. Dunitz and L. E. Orgel, J. Phys. Chem. Solids **3**, 20 (1957).
[51] H. A. Kramers, Physica **1**, 182 (1934).
[52] P. W. Anderson, Phys. Rev. **79**, 350 (1950).
[53] G. W. Pratt, Phys. Rev. **97**, 926 (1955).
[54] J. H. Van Vleck, Electric and Magnetic Susceptibilities, London, Oxford, 1932, p. 311.
[55] L. E. Orgel, J. Chem. Phys. **93**, 1819 (1955).
[56] E. O. Wollan, Phys. Rev. **117**, 387 (1960).
[57] Wilkinson, Gingrich, and Shull, J. Phys. Chem. Solids **2**, 289 (1957).
[58] Cloud, Jarret, Austin, and Adelson, Phys. Rev. **120**, 1969 (1960).
[59] C. Kittel, Phys. Rev. **120**, 335 (1960).
[60] H. Palevsky and D. J. Hughes, Phys. Rev. **92**, 202 (1953), G. L. Squires, Proc. Phys. Soc. (London), **67**, 248 (1954).
[61] A. N. McReynolds and T. Riste, Phys. Rev. **95**, 1161 (1954).
[62] L. Van Hove, Phys. Rev. **95**, 249, 1374 (1954).
[63] F. Zernike and J. Prins, Z. Phys. **41**, 184 (1927).
[64] R. J. Elliot and W. Marshall, Revs Modern Phys. **30**, 75 (1958).
[65] P. G. de Gennes and J. Villain, J. Phys. Chem. Solids **13**, 10 (1960).
[66] M. Erikson and B. Jacrot, J. Phys. Chem. Solids **13**, 235 (1960).
[67] T. Riste, J. Phys. Chem. Solids **17**, 308 (1961).
[68] T. Riste and A. Wanic, J. Phys. Chem. Solids **17**, 318 (1961).
[69] M. K. Wilkinson and C. G. Shull, Phys. Rev. **103**, 516 (1956).
[70] D. J. Hughes, Neutron Optics, Interscience, New York, 1954.
[71] Hughes, Burgy, Eller, and Wallace, Phys. Rev. **75**, 565 (1949).
[72] M. Slotnik, Phys. Rev. **83**, 1226 (1959).
[73] W. L. Roth, J. App. Phys. **31**, 2000 (1960).
[74] W. L. Roth, Acta Crystallogr. **13**, 140 (1950).
[75] Gersch, Shull, and Wilkinson, Phys. Rev. **103**, 525 (1956).
[76] F. Bloch, Z. Physik **61**, 206 (1930).
[76a] Akhiezer, Bar'yakhtar, and Kaganov, UFN **71**, 533 (1960) and **72**, 3 (1960), Soviet Phys. Uspekhi **3**, 567 (1961) and **3**, 661 (1961).
[77] D. I. Blokhintsev, Osnovy kvantovoĭ mekhaniki (Principles of Quantum Mechanics), Moscow, Gostekhizdat, 1940, p. 536.
[78] G. Avakyants, JETP **18**, 444 (1948).
[79] R. G. Moorhouse, Proc. Phys. Soc. **A64**, 1097 (1951).
[80] R. J. Elliot and R. D. Lowde, Proc. Roy. Soc. **A230**, 73 (1955).
[81] R. J. Seeger and E. Teller, Phys. Rev. **62**, 37 (1942).
[82] H. Kaplan, Phys. Rev. **86**, 121 (1952).
[83] S. V. Vonsovskii and Yu. M. Seĭdov, Izv. AN SSSR **18**, 319 (1954), Columbia Tech. Transl. p. 14.
[84] T. A. Kaplan, Phys. Rev. **109**, 782 (1958).
[85] Kondorskii, Pakhomov, and Shiklosh, DAN SSSR **109**, 931 (1956), Soviet Phys. Doklady **1**, 501 (1957).
[86] T. Van Vleck, Revs. Modern Phys. **30**, 1 (1958).
[87] S. V. Maleev, JETP **33**, 1010 (1957), Soviet Phys. JETP **6**, 776 (1958).
[88] F. J. Dyson, Phys. Rev. **102**, 1217, 1230 (1956).
[89] B. N. Brockhouse, Phys. Rev. **106**, 859 (1957).
[90] B. N. Brockhouse, Can. J. Phys. **33**, 889 (1955).
[91] B. N. Brockhouse and A. T. Stewart, Phys. Rev. **100**, 756 (1955).
[92] Riste, Blinowski, and Janik, J. Phys. Chem. Solids **9**, 153 (1959).
[93] R. N. Sinclair and B. N. Brockhouse, Phys. Rev. **120**, 1638 (1960).
[94] R. F. Soshoo, Phys. Rev. **120**, 1978 (1960).
[95] Éntsiklopediya metallofiziki (Encyclopedia of Metal Physics), Moscow-Leningrad 1937, p. 294.
[96] P. R. Pallister, J. Iron Steel Inst. **161**, 87 (1949).
[97] N. G. Backlund, J. Phys. Chem. Solids **20**, 1 (1961).
[98] Legvold, Spedding, Barson, and Elliot, Revs. Modern Phys. **25**, 129 (1953).
[99] Curry, Legvold, and Spedding, Phys. Rev. **117**, 953 (1960).
[100] Hall, Legvold, and Spedding, Phys. Rev. **117**, 971 (1960).
[101] T. Kasuya, Progr. Theor. Phys. Japan **16**, 58 (1960).
[102] B. R. Coles, Suppl. Philos. Mag. **7**, 40 (1958).
[103] G. S. Andersen and S. Legvold, Phys. Rev. Lett. **1**, 322 (1958).
[104] R. J. Weiss and A. S. Marotta, J. Phys. Chem. Solids **9**, 302 (1959).
[105] L. Néel, Z. Elektrochem. **45**, 378 (1939).
[106] C. Zener, Phys. Rev. **81**, 440 (1951).
[107] P. G. de Gennes and J. Friedel, J. Phys. Chem. Solids **4**, 71 (1958).
[108] Mattios, Shul, and Corenzwitt, Phys. Rev. Lett. **1**, 92 (1958).
[109] D. A. Evtushenko and R. Z. Levitin, FMM (Physics of Metals and Metallography) **12**, 155 (1961).
[110] Yu. A. Izyumov, ibid **11**, 801 (1960).
[111] M. A. Ginzburg, FTT **2**, 913 (1960), Soviet Phys. Solid State **2**, 833 (1960).
[112] Sh. Sh. Abel'skii and E. A. Turov, FMM **10**, 801 (1960).
[113] A. A. Berbyshev and I. N. Vlasov, FMM **10**, 628 (1960).
[114] V. L. Bonch-Bruevich, FTT **1**, 186 (1959), Soviet Phys. Solid State **1**, 166 (1959).
[115] B. V. Karpenko, FMM **10**, 794 (1960).

Translated by J. G. Adashko